Università degli Studi di Roma Tre

Faculty of Engineering

Dipartimento di Scienze dell'Ingegneria Civile - DSIC

Scuola Dottorale in Scienze dell'Ingegneria Civile

PhD Thesis

Analytical modeling of flow and transport in highly heterogeneous anisotropic porous formations

Candidate:
Antonio Zarlenga

Supervisor:
Prof. Aldo Fiori

Coordinator:
Prof. Leopoldo Franco

Ciclo Dottorale XXIV

.

.

Collana delle tesi di Dottorato di Ricerca
In Scienze dell'Ingegneria Civile
Università degli Studi Roma Tre
Tesi n° 35

.

Acknowledgements

I'm really grateful to Prof. *Aldo Fiori*, working with him is an amazing experience.
I thank Prof. *Igor Janković* and Prof. *Gedeon Dagan* for their significant contribute to this work.
I want to thank Prof. *Guido Calenda*, Prof. *Elena Volpi*, and Prof. *Corrado Mancini* who supproted me in this work.
I'm really grateful to *Elisa*
and to my friends, *Claudia*, *Francesca*, *Alessandro*, *Federico*, *Michele*, *Pietro* and the other people with whom I spent my life.
I thank *my Parents* and my *Family*.

.

Sommario

Il flusso e il trasporto in formazioni porose tridimensionali, eterogenee e anisotrope sono studiati mediante lo sviluppo di modelli analitici. Lo scopo del lavoro è l'estensione a formazioni anisotrope del modello Auto-Coerente precedentemente sviluppato per mezzi isotropi (Dagan et al., 2003; Fiori et al., 2003; Fiori et al. 2006). L'approccio Euleriano e Lagrangiano sono utilizzati per lo studio delle proprietà, rispettivamente, del flusso e del trasporto di un soluto inerte. I risultati del modello Auto-Coerente (SC) sono stati comparati con quelli ottenuti attraverso il modello al primo ordine (FO) e con accurate simulazioni numeriche (NS). Il modello FO, in passato, ha fornito le soluzioni analitiche delle statistiche del flusso e del trasporto. Queste soluzioni formalmente valide per varianze della permeabilità $\sigma_Y^2 \ll 1$, non sono estendibili direttamente al campo delle elevate eterogeneità. Nell'approccio SC il mezzo è modellato mediante una formazione Multi-Indicatore (MI), alternativa a quella Multi-Gaussiana propria dei modelli FO. La formazione MI è costituita da un insieme di sferoidi oblati, di permeabilità random K_i distribuiti in una matrice omogenea di permeabilità $\mathbf{K}_0$. L'approssimazione SC consente la soluzione analitica delle equazioni del flusso e del trasporto nella struttura MI e quindi la stima del campo di velocità e delle curve di concentrazione (BTC). La metodologia generale è applicata in questo lavoro a inclusioni con permeabilità distribuita in maniera Log-Normale.

La permeabilità efficace, il campo di velocità e il trasporto di un soluto inerte, sono i tre argomenti affrontati nello studio.

Il confronto con le NS evidenzia come il modello SC fornisca ottime stime della permeabilità efficace per un ampio range di eterogeneità σ_Y^2

e anisotropia f. Il modello FO fornisce una stima accurata della permeabilità efficace limitatamente al suo range di applicabilità ($\sigma_Y^2 \ll 1$), mentre importanti differenze dalle NS si evidenziano per le elevate eterogeneità. L'estensione al campo delle forti eterogeneità del modello FO ipotizzata mediante la congettura di Landau-Matheron non sembra possibile.

Lo studio del flusso è sviluppato mediante la stima dei momenti statistici della velocità. I risultati ottenuti nel campo anisotropo sono coerenti con quelli ottenuti da Fiori et al. (2003) per mezzi isotropi. L'effetto dell'anisotropia si esplica nell'aumento della varianza della componente longitudinale della velocità e nella riduzione delle varianze delle componenti trasversale e verticale. La teoria FO, che prevede una crescita lineare della varianza della velocità con l'anisotropia, conduce generalmente a forti sovrastime. Le stime della skewness e della curtosi evidenziano come la distribuzione della velocità non sia Gaussiana, ad eccezione del campo delle basse eterogeneità. La funzione di autocorrelazione è poco dipendente da σ_Y^2. I risultati del modello SC sono confermati dalle simulazioni numeriche.

Il trasporto è studiato in maniera Lagrangiana mediante le curve di concentrazione (BTC) che coincidono con la distribuzione dei tempi di residenza del soluto all'interno del dominio. Il tempo di residenza t è stimato, secondo l'approssimazione SC, dalla somma dei tempi di residenza t_i all'interno delle singole inclusioni considerate non interagenti. Contrariamente a quanto ottenuto nello studio della permeabilità efficace e delle statistiche della velocità, il confronto con le simulazioni numeriche ha evidenziato che la formulazione anisotropa del modello SC consente una stima accurata delle BTC solo per mezzi debolmente anisotropi poichè invece la scarsa sensibilità delle BTC numeriche all'anisotropia.

Abstract

Flow and transport through three dimensional anisotropic heterogeneous formations are investigated using analytical methods. The aim of the present dissertation is to extend, to the relevant case of anisotropic formations, the Self-Consistent method which was developed in the past for isotropic formations (Dagan et al., 2003; Fiori et al., 2003; Fiori et al. 2006). An Eulerian and a Lagrangian approach is employed, respectively, for the analysis of the properties of the flow and the advective transport of a plume of inert solute. The results obtained by the Self-Consitent (SC) method are compared with those obtained by the well-known First-Order (FO) approach, that, in the last 30 years, has led to several useful analytical solutions on flow and transport statistics. However, such solutions suffer from the strong limitation of weak heterogeneity, i.e. they are formally valid for $\sigma_Y^2 \ll 1$. Accurate numerical simulations (NS) free from model approximations are employed to test the semi-analytical method.

Uniform flow of constant mean velocity takes place in a random hydraulic conductivity field, which is modeled by Multi-Indicator (MI) model alternative to the Multi-Gaussian employed in the FO method. The mean flow direction is aligned with the long axis of anisotropy. The MI formation is made up of a collection of non-overlapping oblate spheroids of random hydraulic conductivity K_i, placed in a matrix of hydraulic conductivity $\mathbf{K}_0$. The SC argument is used to calculate approximate analytical solutions for the velocity field and the breakthrough curves. The methodology is applied to a medium with inclusions of normally distributed logpermeability $Y = lnK$.

The thesis is organized into three sections, investigating the effective properties of the medium, the flow, and the transport .

The main contribution to the study of the effective conductivity lies in the comparisons between the results of the analytical models with the numerical simulations. It is found that the SC solution is very accurate for a broad range of the values of heterogeneity and anisotropy (f). The FO approximation provides a good estimation of the $\mathbf{K}_{ef}$ in its range of applicability ($\sigma_Y^2 \ll 1$), but strongly deviations from the numerical simulations are observed for large σ_Y^2. The extension of the first order results to high heterogeneous media is not possible by using the exponential Landau- Matheron conjecture.

The study of the flow is conducted through the evaluations of the statistical moments of the velocity. Closed-form expressions for both average velocity and its variance were obtained, while higher order moments (up to fourth), velocity autocorrelation and integral scales are computed by numerical quadratures. If anisotropy is absent, the solutions converge to those developed for isotropic media by Fiori et al. (2003). The main effect of anisotropy is to increase the variance of the longitudinal velocity and to reduce the variances of the transverse and vertical components. Surprisingly, the growth of the vertical velocity variance with heterogeneity (σ_Y^2) is not always monotonous. FO solutions generally overpredict the growth trends of the velocity variance with heterogeneity. Analysis of skewness and kurtosis suggests that the velocity probability density function (pdf) is generally far from Gaussian, except for weakly heterogeneous formations. The deviation from Gaussianity increases with increased anisotropy for all velocity components. The velocity autocorrelation function is weakly dependent on σ_Y^2, as confirmed by the numerical simulations.

Transport is analyzed in terms of breakthrough curve (BTC) of the solute, identical to the traveltime distribution, at a control plane at distance x from the source. The global traveltime t is evaluated through the SC

approximation by summing residence times in the inclusions t_i.

The anisotropic formulation of SC model is not able to reproduce numerical simulations. The SC method proves its ability to provide adequate estimation of the BTCs only in low anisotropic domains. These results are not in accordance with the ones concerning the effective conductivity and the velocity statistics.

.

Contents

List of Figures

Symbols

$\langle ... \rangle$	Expected value
$\widehat{\ }$	Fourier transform
Superscript $'$	Denoted fluctuation of a SRF from its expected value
C	Phase concentration
C_Y	Covariance of the SRF Y
C_{HY}	Cross-Coveriance between $Y(\mathbf{x})$ and $H(\mathbf{x}')$
C_H	Covariance of the SRF H
$D_{i,j}$	Macrodispersion tensor
e	Spheroid eccentricity
f	Integral-Scale ratio (Anisotropy)
I_Y	Y Integral scale
I	Indicator function
$I_{Z,i}$	Integral scale of Z in the $i-th$ direction
J_i	Negative mean head gradient in the $i-th$ direction
K	Hydraulic conductivity
$\mathbf{K}ef$	Effective hydraulic conductivity
$\mathbf{k}$	Wave number vector
k	Hydraulic conductivity ratio
H	Hydraulic head
n	Inclusion density

$p_Z(z)$	Probability distribution function of z
q	Specific discharge
R	Spheroid semi-axis
$\mathbf{r}$	Separation distance vector
t	Time or Traveltime
U	Mean velocity
u	The deviation of the velocity from its expected value
$u_{i,j}$	Velocity covariance
V	Fluid velocity
$\mathbf{X}_t$	Particle trajectory (displacement function)
$X_{i,j}$	Covariance of the particle trajectory
$\mathbf{x} =(x_1, x_2, x_3)$	Cartesian coordinate vector
$\overline{\mathbf{x}}$	Spheroid centroid
x	Domain longitudinal dimension
Y	Log-conductivity

δ	Dirac's delta
γ_Y	Semivariogram of the SRF Y
θ	Effective porosity
μ	Solute fulx
ρ_Y	Correlation of the SRF Y
σ_Y^2	Variance of the SRF Y (Heterogeneity)
σ_u^2	Variance of the velocity
τ	Traveltime residual
ϕ	Flow potential
φ	Flow potential disturbance
$\chi(r)$	Overlap function
Ω	Flow domain
ω	Spheroid volume
ω'	Speroid rejection zone
(ζ, η, ψ)	Oblate spheroidal coordinate vector

.

Chapter 1

Introduction

Stochastic modeling of subsurface flow and transport was developed in the last 35 years and is now a common and advanced approach for the study of the subsurface hydrology. This approach implies that the hydrological variables and parameters are affected by uncertainty and regards them as random variables. this basic idea is not new, and was adopted in many disciplines, among which surface hydrology.

In the study of subsurface processes the principal source of uncertainty is the spatial variability of the hydraulic properties. The physical processes which are the object of the study occur in a medium characterized by random properties and hence the physics of the phenomena is described by stochastic constitutive equations and by stochastic differential equations of flow and transport. The solute transport through an aquifer, like a porous formations, depends on many factors, and reflects the natural complexity of the medium, which is typically heterogeneous and anisotropic. Great difficulties occur when this study involves real-scale field experiments. Tridimensional reconstruction of the concentration field requires many measure points; the

observing time must be congruent with the temporal evolution of natural process characterized by slow dynamics; consequently data acquisition should be very accurate, protracted for long time and hence very expensive. Theoretical researches and physically based models are the principal tools to understand this natural media and to identify the most significant factors in flux and solute transport.

Following the classification coined by Dagan, each groundwater model is characterized by three length scales, which characterize respectively the medium, the flow and the transport processes.

I-The first scale, L, is associated to the extension of the flow domain. Tree possibility can be recognized as representative for L: laboratory, local and regional.

The laboratory scale pertains to the sample, his extension is less than 1 m and heterogeneity is associated with the network of solid-void pore structure. When carryng out a study at local scale the medium can be considered homogeneous and the flux can be considered as monodimensional.

The local formation scale dimensions of the domain are related to the thickness of the aquifer (and to similar dimensions in the plane) and the characteristic length is 10-100 m. At this scale heterogeneity is associated with the spatial variations of permeability, the medium must be considered as non-homogeneous and potentially anisotropic, hence flow phenomena are typically three dimensional.

Finally the regional scale pertains the entire aquifer, the domain planar dimension ($>$ 1000 m) is much larger than its thickness, the heterogeneity is associated to the variations of the trasmissivity while the flux can be considered as bidimensional.

II-The second fundamental scale, I, is that associated with the spatial

heterogeneity of the hydraulic properties. I, is the distance at which hydraulic properties can be considered uncorrelated. I is determined directly or indirectly frommeasurements by using geostatistical inference thecniques.

III-The third fundamental scale, D, characterizes the volume over which the variable or properties are averaged (elementary volume). For example at laboratory scale D is the dimension of the cross section over which the data are averaged.

The hierarchy of the scale plays a crucial role. Thus at laboratory scale $I \ll D \ll L$, at regional scale is quite often $D \ll I \ll L$ whereas at local scale the order are less definite.In the groundwater modeling basic assumptions are that $I \ll L$ and that statistical stationarity holds. These two assumptions are necessary in order to infer the statistical structure of the random function describing heterogeneity from a single available realization.

In this work we present work is a theoretical study of the flow and transport at local scale in highly heterogeneous and anisotropic formations. Our first aim is a theoretical analysis of the flux and transport processes, to better undestand the nature of physical phenomena which are indirectely observed through field experiments. Our second (practical) interest is to provide a useful tool for the applications in groundwater engineering that require not only the mean fluxes but also a forecast of the second order moments or a more accurate prediction of the transport process. Research is built on conceptual models of formation heterogeneity. Darcy law and mass balance equations are solved analytically or semi-analytically to carry out

- the effective hydraulic conductivity,
- the statisitcal moments of velocity field,
- the solute flux through a specified section of the flow domain.

Two models are compared: the first one based on the solutions of the flow

and trasport equations in the medium, modeled through a Multi-Indicator (MI) formation and the second one based on the direct solution of the stochastic equations using perturbations expansion, in a multivariate normal medium. The first model, recently developed, allows the study of high heterogeneous random media, being ahead of the limit of low-heterogeneity of the secon method. Second method is known as First Order Approximation (FOA) and around it a huge body of literature was developed in the last 30 years. This model has done a fundamental contribute to developing the stochastic subsurface hydrology, but its application is limited to low-heterogeneity formations.

The principal effort of this research consists in extending the solution, of the MI model, provided by Dagan, Fiori and Janković (Dagan and Fiori, 2003, Fiori and Dagan, 2003, Dagan et al., 2003, Fiori et al., 2003, Janković et al., 2003, Fiori et al., 2006, Janković et al., 2006.) from isotropic medium to anisotropic medium. Analytical or semi-analytical results are tested with accurate numerical simulations obtained by Prof. Igor Janković using the procedure described in Janković et al., 2003 and in Suribhatla et al. 2011.

1.1 Organization of the Research

In chapter 2 the stochastic characterization of the porous formations is described. In Chapter 3 the mathematical structures of the methods Sel-Consistent and First-Order and FO are described. Chapter 4-5-6 are dedicated, to the study, respectively, of the effective hydraulic conductivity, of the flow statistics and of the solute transport. In chapter 7 the research results are summarized.

Chapter 2

Stochastic aquifer characterizations

Before applying concepts of probability and stochastic modeling to groundwater applications it is important to understand the physical meaning of interpreting formation heterogeneity as probabilistic. In a strict sense, natural formations do not qualify as probabilistic experiments with unknown outcomes and hydraulic conductivity is a deterministic phenomenon i.e. their measurement yields the same values at the same point if the same method is used and if measurement errors are neglected. The rationale for a stochastic framework is justified by considering natural formations as an experiment that has been performed already, but the outcome is not known since it has not been observed or measured. Adopting the stochastic modeling framework involves assumptions on the statistical nature of formation heterogeneity. In this Chapter, the various assumptions used in this study and the statistical parameters for describing spatially varying hydraulic conductivity are presented.

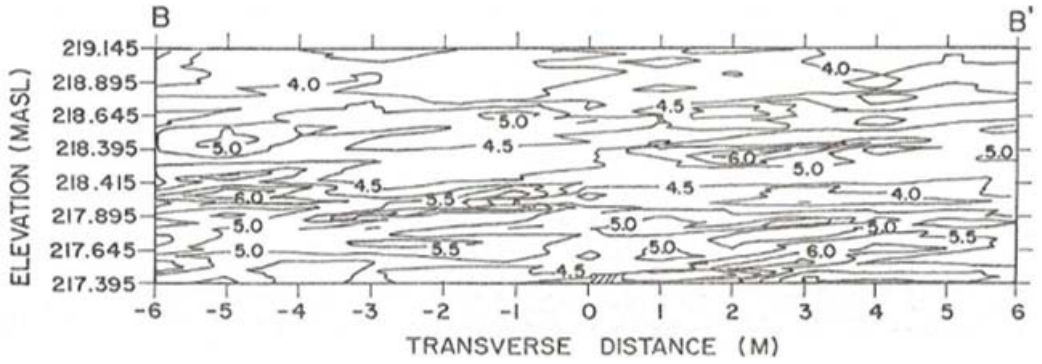

Figure 2.1: Lines of constant -log K (K in cm/s)in a vertical cross-section at the Borden tracer site test. From Sudicky, (1986) in Dagan, (1989).

Natural porous formations are constituted naturally by predominantly horizontal layers. Each layer has its own hydraulic (and mechanics etc.) characteristics. This complex structure is a consequence of the natural process of deposition. At the formation scale, it is often impractical to collect the large set of hydraulic conductivity data necessary to simulate deterministically the processes of flow and transport that occur in the medium; Figure 2.1 shows the hight variability of the log-conductivity extimated in a cross section at the Borden site. For example Rehfeldt et al. (1992) estimated that 400000 hydraulic conductivity measurements would be needed to create a deterministic groundwater model for the Macrodispersion Experiment site at *Columbus Air Force Base* in Mississippi (MADE). As noted by many authors, this heterogeneity is very complex and difficult to describe quantitatively on a point by point basis and restricts our ability to construct deterministic models.

Alternatively, this variation and uncertainty in the local scale hydraulic conductivity can be modeled using space random functions (SRFs). A stochas-

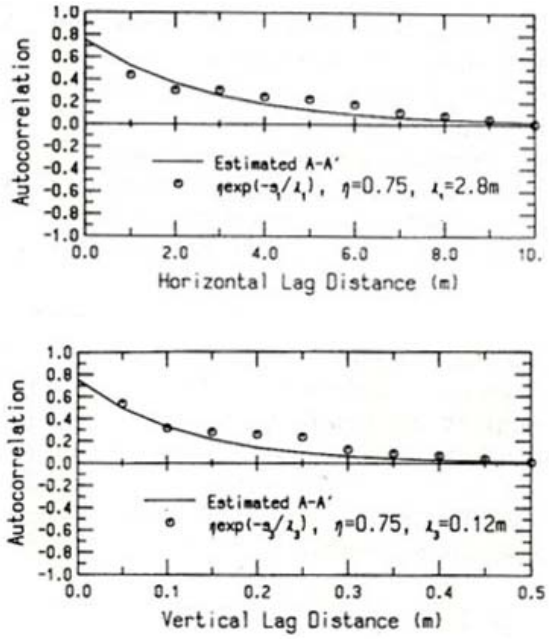

Figure 2.2: Hydraulic conductivity autocorrelation in the horizontal and in the verical direction at the Borden tracer site test. From Sudicky, (1986) in Dagan, (1989).

tic approach allows, for systematic way, of accounting for the uncertainty and spatial variability in the independent parameters (in this dissertation hydraulic conductivity) by treating them as a collection of random variables. The permeability field is regarded hence as only one possible realization.

This innovative approach was introduced by Freeze (1975) in his pioneer study, where he attempts to summarize hydraulic conductivity field data K from literature. His first finding was that $K(\mathbf{x})$ varies in irregular manner and the best fit is achieved by using a lognormal distribution. Now it is common to assume that Y values at an arbitrary set of points is multi-variate normally distributed, but such a choice is not warranted (see discussion in

Gómez-Hernández et Wen, (1996) and in Janković et al., (2003).

Field studies also indicate that sedimentary aquifers typically exhibit an anisotropic behaviour, where K has stronger correlation in horizontal direction and weaker correlation in the vertical direction. Field observations show that the integral scale $\mathbf{I}_Y$, the maximum distance at which two point can be considered uncorrelated $\sim$ 1 m in the horizontal direction and $\sim$ 1 in the vertical direction. Figure 2.2 shows the autocorrelation function extimated for the Borden site.

If we assume $Y = log(K)$ being normal distributed the complete characterization of the hydraulic conductivity field is achieved by the mean $\langle Y \rangle$, the variance σ_Y^2 and the covariance function $C_Y(\mathbf{x})$. The first two parameters are referred to statistics of Y while C_Y represents spatial continuity of hydraulic properties. It is important to clarify that at local scale anisotropy manifests itself through the shape of the covariance function while the conductivity tensor is locally isotropic. The shape of the covariance function reflects the geometric properties of the natural porous formations. Such media are modeled by representing the log-conductivity two-point covariance as axi-symmetric, of two different correlations scales I_{Yh} and $I_{Yv} = fI_{Yh}$, in the horizontal plane and vertical direction, this results are quite general as confirmed from many authors (see for example, Rubin, 2003, Tab 2.2)

In groundwater applications at local scale, the first task is accomplished by performing a geostatistical analysis on the data collected and estimating the statistical properties of the permeability field.

2.1 Hydraulic Conductivity: a Space Random Function

A random function is a set of random variables: with many values in one particular realization or a random vector with many components in each realization. A random vector is either defined by the joint probability density function (pdf) of all the components, or by having a set of all possible realizations of the random vector from which a probability distribution function can be constructed. In stochastic subsurface modeling, measurements of hydraulic conductivity (K) at various locations can be defined as a random experiment and the examined aquifer as a single realization of a spatial stochastic process. Using a finite number of measurements and simplifying assumptions, the space random function representing hydraulic conductivity can be described satisfactorily. The aim of the procedure is usually not to obtain a joint probability density function but to derive few statistical parameters ($\langle Y \rangle$, σ_Y^2, I_Y, $C_Y(\mathbf{x}', \mathbf{x}'')$) quantifying the spatial structure.

The random function $Y(\mathbf{x})$ represents the spatially varying hydraulic conductivity, where $\mathbf{x} = (x_1, x_2, x_3)$ is the three-dimensional spatial coordinate. The operational usefulness of this transformation is in view of numerous field studies that have suggested that measurements of K follow a univariate lognormal distribution (Y) is a normal variable) and is the starting point for further analysis as found in standard textbooks on stochastic subsurface modeling (e.g. Dagan (1989), Rubin (2003)). In this study also, the univariate conductivity pdf is treated as log-normal. As discussed previously, $p(Y(\mathbf{x}))$ is practically impossible to determine and only a few measurements $Y(\mathbf{x}')$, $Y(\mathbf{x}'')$, ... are available from one realization (we can examine only the actual aquifer) to describe the entire stochastic process. Following this lim-

itation, the spatially varying K is treated as a SRF and certain assumptions are made about the stochastic process underlying its variability.

The main assumption made here is of a statistically simpler medium: the spatial stochastic process is 2th order stationary. For a statistically homogeneous (stationary) formation, the univariate mean $\langle Y(\mathbf{x})\rangle$, variance $\sigma_Y^2(\mathbf{x})$ are finite and independent of the location $\mathbf{x}$ and the 2-point correlation or 2-point covariance $C_Y(\mathbf{x}', \mathbf{x}'')$ is only a function of the separation distance $r = |\mathbf{x}' - \mathbf{x}''|$.

$$\begin{aligned} \langle Y(\mathbf{x})\rangle &= \langle Y\rangle \\ \sigma_Y^2(\mathbf{x}) &= \sigma_Y^2 \\ C_Y(\mathbf{x}', \mathbf{x}'') = \langle (Y(\mathbf{x}') - \langle Y\rangle)(Y(\mathbf{x}'') - \langle Y\rangle)\rangle &= C_Y(r) \end{aligned} \tag{2.1}$$

A standard notation is adopted here, angled brackets denote ensemble averages of the term inside the brackets. The parameter $\langle Y\rangle$ is the logarithm of geometric mean K_G of the conductivity values.

In geostatistics it is common to use a semi-variogram Y (e.g. Kitanidis, 1989) instead of the covariance to represent the structure. The formal definition of semi-variogram is,

$$\gamma_{_Y}(r) = \frac{1}{2}\left\langle (Y(\mathbf{x}) - Y(\mathbf{x}+\mathbf{r}))^2 \right\rangle \tag{2.2}$$

and can be used as a measure of dissimilarity. For a 2th order stationary process $\gamma_{_Y}(r)$ is directly related to the covariance as

$$\gamma_{_Y}(r) = \sigma_Y^2 - C_Y(r) \tag{2.3}$$

Common types of experimental models used to infer this function from measurements include semi-spherical, nugget, exponential and gaussian models (see e.g. Kitanidis, (1997), Dagan, (1989), Rubin (2003)) among others.

The parameters that define the spatial correlation succinctly are the integral scales $\mathbf{I}_Y$. The formal definition of the integral scale for a three-dimensionally anisotropic (general) medium is

$$I_{Y_i} = \frac{1}{\sigma_Y^2} \int_0^\infty \rho_Y(x_i) dx_i \qquad i = 1, 2, 3 \tag{2.4}$$

where $\rho_Y(\mathbf{x}) = C_Y(\mathbf{x})/\sigma_Y^2$ is the autocorrelation function of the logpermeablity Y, and can be understood as the separation distance below which two values are fully correlated.

Stochastic processes that do not have constant and finite values for either or all of mean, variance and integral scales might exhibit an ever-increasing scale of variability and are by definition non-stationary or evolutionary. This study is limited to formations that are characterized by finite mean and variance of Y and a well-defined integral scale, $\mathbf{I}_Y$ such as the Cape Cod or Borden aquifers, following the main assumption of stationarity.

.

Chapter 3

Matematical statement

The formulation of the direct flow problem is as follows: given the flow domain and the formation properties, derive the specific discharged and the velocity. In this dissertation, on the flow and transport at local scale, the domain Ω is defined by a 3D channel consituted by a saturated porous formation. We neglect the elastic storage and the recharge, water flow in the porous medium is governed hence by Darcy's law and continuity, that for a incompressible fluid in steady state are. In this dissertation, we consider mean uniform flow, of constant mean velocity $\mathbf{U}$, in a large domain Ω. Mean velocity $\mathbf{U}$ is aligned with x_1, the longitudinal coordinate, while x_2, x_3 are the lateral and vertical coordinates, respectively. Water flow in the porous medium is governed by Darcy's law and continuity

$$\mathbf{q} = -K\,\nabla H \;\; ; \quad \nabla \cdot \mathbf{q} = 0 \qquad (\mathbf{x} \in \Omega) \tag{3.1}$$

where $\mathbf{x}\,(x_1, x_2, x_3)$, $\mathbf{q}$ is the specific discharge, H the pressure-head and K is the hydraulic conductivity. We assume that the effective porosity θ is constant and therefore $\mathbf{V} = \mathbf{q}/\theta$ is proportional to the fluid velocity and we shall denote it as either flux or velocity in the sequel. In the deterministic

case, dependent variables, head and specific discharge vector $\mathbf{q} = (q_1, q_2, q_3)$, are solved for a given conductivity (K) and boundary conditions. In the stochastic approach, since $Y(\mathbf{x})$ is modeled as a SRF, the dependent variables are also random variables. Hence, the methods of solving eqs (3.1) is aimed at deriving their statistical moments or preferably their pdfs.

We assume the hydraulic conductivity field $K(\mathbf{x})$ or $Y(\mathbf{x}) = \ln K(\mathbf{x})$, as random and stationary with Y normal, of two-point covariance $C_Y(\mathbf{x}, \mathbf{y}) = \sigma_Y^2 \rho_Y(r)$, $r = |\mathbf{x} - \mathbf{y}|$, with σ_Y^2 and ρ_Y the variance and the autocorrelation function, respectively. Following field data (see, e.g., Rubin, 2003) and literature studies we model sedimentary aquifers by using an axisymmetric autocorrelation function which is obtained by inserting $r' = [(r_1^2 + r_2^2)/I_h^2 + r_3^2/I_v^2]^{1/2}$ into an isotropic autocorrelation function $\rho_Y(r')$. Here $I_{Yh} = \int_0^\infty \rho_Y(r_1, 0, 0)\, dr_1 = \int_0^\infty \rho_Y(0, r_2, 0)\, dr_2$ and $I_{Yv} = \int_0^\infty \rho_Y(0, 0, r_3)\, dr_3$ are the horizontal and vertical logconductivity integral scales, respectively. Thus, at second-order the stationary structure is characterized entirely by the four parameters $K_G = \exp\langle Y \rangle$, σ_Y^2, I_{Yh} and f, where $f = I_{Yv}/I_{Yh}$ is the anisotropy ratio (generally $f < 1$) and K_G is the geometric mean of K.

Complete statistical characterization requires the knowledge of various multipoint autocorrelations besides the two-point one, but multipoint autocorrelations are usually not identifiable from field data because of their scarcity.

3.1 The Stochastic Framework for Modeling

Two analytical methods are investigated:

I-The direct solution of the stochastic governing equations through perturbation expansion thecnique: the solution is developed on the assumption

of Y stationary and multivariate normal with generic covariance structure. This method described in the following section can be applyed only to low heterogeneity fields. Experiments of Borden and Cape Code have shown that this theory is not able to explain characteristic physical phenomena of highly heterogeneous formations.

II-The approximate solution of the flow and transport equations through a Multi-Indicator (MI) formation: the porous medium is modeled as a collection of nonoverlapping spheroids of independent random conductivities $K = \exp(Y)$, embedded into a homogeneous matrix of conductivity K_0. Suribhatla et al. (2011) developed an efficient and accurate numerical procedure for the solution of the flow problem for this model that requires, however, intensive computational resources.

Movement of groundwater in statistically anisotropic formations can be significantly different from that in isotropic aquifers. In view of the limitations of traditional stochastic methods, the Multi-Indicator Model provides an ideal framework for studying flow and transport characteristics of anisotropic formations. The approximate solutions shall be compared with the results of numerical simulations carry out by using the procedure developed in Suribathla et al. (2011).

3.2 First-Order Approximation

In this chapter we recall briefly the well-known solution of the stochastic equations for flow and transport solved by perturbative methods. A big body of litterature was developed in the last 30 years after the fundamental works Gelhar, 1983, and Dagan, 1984 and 1987. The theroy known as First-Order approximation (FOA) is, at this moment, the reference theory in the advanced study of groundwater.

Here a is presented a brief remind to the hypothesis and the general lines of first-order solution, the complete theory constitutes a big body of literature and all the aspects can not discussed here, but they are avaialable in the monographs Dagan, 1989, Gelhar, 1993 and Rubin 2003, interesting advanced issues are Fiori, 1996, Fiori and Dagan, 1999, Fiori et al. 2002, and Russo, 1995 and 1998.

The main aim to this theory is to relate the concentration field to the characteristic of aquifers that can be estimated by the collected field data ($\langle Y \rangle$, $C_Y(r)$).

The starting point of the mathematical solution is the continuity and Darcy equations (3.1), standing the relation $\nabla K/K = \nabla lnK = \nabla Y$ we can write

$$\nabla^2 H + \nabla Y \nabla H = 0 \tag{3.2}$$

We write the logconductivity at first order as the summation of its mean value and its fluctuation,

$$Y = \langle Y \rangle + Y' \quad , \quad \langle Y' \rangle = 0 \quad i.e. \tag{3.3}$$

hence eq (3.2) becomes

$$\nabla^2 H + \nabla Y' \nabla H = 0 \tag{3.4}$$

The small perturbation method require a small parameter; we focus our attention on with small hydraulic conductivities fluctuation Y', and hence small σ_Y. We expand the variable H in

$$H = H^{(0)} + H^{(1)} + H^{(2)} + ... \tag{3.5}$$

generic $i-th$ term of the previous series is of the same order of $(\sigma_Y)^i$. Inserting eq (3.5) in eq (3.4) and collecting the terms of the same order we obtain for $n \leq 1$

$$\begin{array}{ll} n=0 & \nabla^2 H^{(0)} = 0 \\ n=1 & \nabla^2 H^{(1)} = -\nabla Y' \nabla H^{(0)} \end{array} \tag{3.6}$$

We assume as boundary conditions a deterministic gradient applied at infinity. The $0-th$ order correspond to the deterministic problem, taking the expectation on the first equation ($n=0$) we obtain the first relation:

$$\left\langle H^{(0)} \right\rangle = H^{(0)} = \mathbf{J}\mathbf{x} \tag{3.7}$$

By multiplying both sides of the second relation ($n=1$) in eq (3.6) by $Y'(\mathbf{x}')$ we obtain

$$Y' \nabla^2 H^{(1)} = -Y' \nabla Y' \nabla H^{(0)} \tag{3.8}$$

taking the expected value, standing $J_i = \partial H_0 / \partial x_i$, we obtain (for details see Dagan, 1989)

$$\nabla_x^2 C_{Y,H}(\mathbf{x}', \mathbf{x}) = J_i \cdot \nabla_x C_Y(\mathbf{x}', \mathbf{x}) \tag{3.9}$$

We recall the 2th order stationarity and defininig $r = |\mathbf{x}' - \mathbf{x}|$ we obtain

$$\nabla_x^2 C_{Y,H}(r) = J_i \nabla_r C_Y(r) \tag{3.10}$$

Multiplying the relation (3.8) evauated in $\mathbf{x}'$ and the same relation evaluated in $\mathbf{x}''$ and tacking expected value we obtain the foundamental relation

between the head gradient and the covariance structure of the medium

$$-J_i J_j \frac{\partial^2 C_Y(\mathbf{x}', \mathbf{x}'')}{\partial x_i' \partial x_j''} = \nabla_r^2 \nabla_r^2 C_H(\mathbf{x}', \mathbf{x}'') \tag{3.11}$$

where $J_i$is the deterministic gradient applyed as boundary condition, $C_Y(\mathbf{x}', \mathbf{x}'')$ is the logconductivity field covariance and $C_H(\mathbf{x}', \mathbf{x}'')$ is the head covariance at first-order depending both on the 2-point distance $r = |\mathbf{x}' - \mathbf{x}''|$. The last equality constitutes the fundamental relation between the head random fiel covariance and the hydraulic conductivity covariance.

Velocity at first-order is obtained from the Darcy law as

$$\begin{aligned} \mathbf{V} &= -\tfrac{1}{n} \exp(Y) \nabla H = \\ &= -\tfrac{1}{n} \exp(\langle Y \rangle)(1 + Y') \nabla (H + H') = \\ &= \tfrac{1}{n} \exp(\langle Y \rangle)(1 + Y') \nabla (\mathbf{J}\mathbf{x} - H') \end{aligned} \tag{3.12}$$

where the prevoius notation $H^{(1)}$has been repalced with H'; V as Y and H consists of terms proportional to different powers of Y' (or σ_Y) hence the velocity can be viewed as the series

$$\mathbf{V} = \mathbf{V}^{(0)} + \mathbf{V}^{(1)} + \mathbf{V}^{(2)} ...; \quad \mathbf{V}^{(i)} \sim \sigma_Y^i \tag{3.13}$$

collecting the terms of order equal to 1 we obtain

$$\mathbf{V}^{(1)} = u = \frac{1}{n} \exp(\langle Y \rangle)(\mathbf{J} Y' - \nabla H') \tag{3.14}$$

After some algebraic passages previous equation lead to the final fundamental expression that connect, in the Fourier space the velocity covariance and the conductivity field covariance (see for more details Dagan, 1989 or Gelhar, 1993):

$$\widehat{u}_{i,j} = U_p U_q \left(\delta_{p,i} - \frac{k_i k_p}{k^2} \right) \left(\delta_{q,j} - \frac{k_j k_q}{k^2} \right) \widehat{C_Y} \tag{3.15}$$

where δ is the identity matrix and $k = \sqrt[2]{k_3^2 + k_3^2 + k_3^2}$.

The study of the transport is approached by lagrangean framework. We focus our attention in the particle of mass ΔM_0 that occupies a small volume in the flow field. $X(t)$ is the trajectory that defines the particle position at time t as function of its initial position at time t_0

$$\mathbf{X}(t|\mathbf{a}, t0) = \mathbf{a} + \int_{t_0}^{t} \mathbf{V}(t'|\mathbf{a}, t_0)dt' \tag{3.16}$$

Standing the randomness of V the particle trajectory is a random function and it can be associated with its mean and covariance

$$\begin{gathered}\langle \mathbf{X}(t|\mathbf{a}, t0)\rangle = \mathbf{a} + \left\langle \int_{t_0}^{t} \mathbf{V}(t'|\mathbf{a}, t_0)dt' \right\rangle \\ X_{i,j}(t|\mathbf{a}, t0) = \langle (X_i(t|\mathbf{a}, t0) - \langle X_i(t|\mathbf{a}, t0)\rangle)(X_j(t|\mathbf{a}, t0) - \langle Xj(t|\mathbf{a}, t0)\rangle)\rangle\end{gathered} \tag{3.17}$$

Neglecting the pore-scale dispersion the fluctuations of the Lagrangean velocity about its mean is defined by

$$\mathbf{V}' = \mathbf{V} - \langle \mathbf{V}\rangle \tag{3.18}$$

the fluctuation of $\mathbf{X}(t|a, t0)$ about its mean is related to the previous equation by

$$\mathbf{X}'(t) = \mathbf{X}(t) - \langle \mathbf{X}(t)\rangle \tag{3.19}$$

Substituing eqs (3.18) and (3.19) in eq (3.17a) we obtain the following relations that relate the mean and the fluctuation of the velocity with the meand and the fluctuation of the displacement

$$\begin{gathered}\langle \mathbf{X}(t)\rangle = \mathbf{a} + \int_{t_0}^{t} \langle \mathbf{V}(t')\rangle \, dt' \\ \mathbf{X}'(t) = \int_{t_0}^{t} \mathbf{V}'(t')dt'\end{gathered} \tag{3.20}$$

The displacement covariance tensor (3.17b) becomes

$$\begin{gathered} X_{i,j}(t) = \left\langle X_i'(t) X_j'(t) \right\rangle = \\ = \left\langle \int_{t_0}^{t} V_i'(t')dt' \int_{t_0}^{t} V_j'(t'')dt'' \right\rangle = \\ = \int_{t_0}^{t} \int_{t_0}^{t} \left\langle V_i'(t') V_j'(t'') \right\rangle dt''dt' = \\ \int_{t_0}^{t} u_{i,j}(t', t'')dt''dt' \end{gathered} \tag{3.21}$$

Previous equations (3.17) and (3.21) relate the flow field statistics with the displacement statistics. A complete stochastical characterization of $X(t)$ requires to define the pdf $p_{X(t)}(\mathbf{x})$. Total displacement is the sum of many small uncorrelated ones, we can invoke the central limit theorem and assert that, at large travel time, $\mathbf{X}(t)$ becomes normal and hence it is exhaustively characterized by its first two moments evaluated. If we assume that the flux is uniform in the mean, with mean flow $\mathbf{U} = (U, 0, 0)$ the $p_{X(t)}(\mathbf{x})$ is

$$p_{X(t)}(\mathbf{x}) = \frac{1}{(2\pi)^{3/2}(X_{11}X_{22}X_{33})^{1/2}} \exp\left(-\frac{1}{2}\left(\frac{(x_1 - Ut)^2}{X_{11}} + \frac{{x_2}^2}{X_{22}} + \frac{{x_3}^2}{X_{33}}\right)\right) \tag{3.22}$$

Let us reconsider a non reactive solute particle of mass ΔM_0 that occupies a volume da of order of magnitude of a few pores. The mass can be written in terms of concentration

$$\Delta M_0 = C_0 \theta_0 da \tag{3.23}$$

If we assume that the volume of the particle remains constant the concentration at any coordinate $\mathbf{x}$ and at any time t is C_0 if $\mathbf{x}$ falls within the volume occupied by the particle at time t and zero otherwise.

$$C(\mathbf{x}, t) = \frac{C_0 \theta_0 da}{\theta} \delta(\mathbf{x} - \mathbf{X}(t|t_0, \mathbf{a})) \tag{3.24}$$

A common assumption is that the porosity n does not change in space the previous equation hence becomes

$$C(\mathbf{x},t) = C_0 da \delta(\mathbf{x} - \mathbf{X}(t|t_0,\mathbf{a})) \tag{3.25}$$

Since $\mathbf{X}$ is random then so is C and it need to be characterized through its statistical moments. The expected value of the concentration is obtained by taking the expected value over the renge of $\mathbf{X}$ values

$$\begin{aligned} \langle C(\mathbf{x},t)\rangle = \textstyle\int_\Omega C_0 da \delta(\mathbf{x} - \mathbf{X}(t|t_0,\mathbf{a})) p_{X(t)}(\mathbf{X}') d\mathbf{X}' = \\ = C_0 \ da \ p_{X(t)}(\mathbf{x}) = \Delta M_0/\theta_0 p_{X(t)}(\mathbf{x}) \end{aligned} \tag{3.26}$$

This fundamental result can be put into words as follows: the expected value of the concentration field ΔC is proportional to the probability distribution function of the particles displacements which originates at $\mathbf{x} = \mathbf{a}$ for $t = t_0$, in which the displacement $\mathbf{X}$ is replaced by the space coordinate $\mathbf{x}$.

The concentration expeced value is is completely determined by the various moments of the displacements $\mathbf{X}(t)$ which characterize $f_{X(t)}$. When $f_{X(t)}$ becomes Gaussian it satisfy the convection-dispersion equation

$$\frac{\partial \langle C\rangle}{\partial t} + \sum_{j=1}^{3} U_j \frac{\partial \langle C\rangle}{\partial x_j} = \sum_{i=1}^{3}\sum_{l=1}^{3} D_{jl} \frac{\partial^2 \langle C\rangle}{\partial x_j \partial x_l} \tag{3.27}$$

where $D_{jl} = 1/2 dX_{jl}/dt$. Neglecting the pore-scale dispersion, the macrodispersion coefficient D_{jl} can be obtained from the eqs (3.21) (3.15). Eq (3.27) is formally equal to the convection-dispersion equation determined at laboratory scale but the meaning is different. D_{ij} is not a simple constant diffusion coefficient, it is time-dependent and it characterize the dispersion phenomena generated by the velocity gradients at local scale. Only for large traveltime D_{ij} tends to a constant value the transport becomes Fickian.

3.3 Multi Indicator Model

General formulation

In this section we recall briefly the definition and the properties of the multi indicator structure. This conceptual model formation was applied for the first time on filtration problems in saturated porous media by Dagan in the 1989. Dagan in the 1989 carrys out an estimation of the effective hydraulic conductivity, subsequently in the 2003 theMI model was developed and applied to the study of statistical properties of flow and transport fields for isotropic structures. In the present dissertation along the guidelines traced in Dagan et al. (2003), Fiori et al. (2003) and (2006) the MI solution is extended to anisotropic formations. This non trivial extension required a complete redefinition of the analytical structure.

Through the MI model the flow domain $\Omega = L_1 L_2 L_3$ is assumed to be made of non-overlapping blocks. Each block $\omega^{(i,k)}$ is homogeneous and isotropic, with random hydraulic conductivity $K^{(i)}$ with $i = 1, 2, ..M$. The probability density function (pdf) of the conductivity of the blocks is assumed lognormal with mean and variance assigned.

We denote as $\omega^{(i,k)}$ the domain or the volume of a single block of hydraulic conductivity $K^{(i)}$ and centroid location $\overline{\mathbf{x}}^{(i,k)}$, with $k = 1, 2..M^{(j)}$. We assume that $\omega^{(i,k)}$ is known, whereas $\overline{\mathbf{x}}^{(i,k)}$ are random variables. We denote as $N = \sum_{i=1}^{M} M^{(i)}$ the total number of the block constituent the flow domain Ω.

The random conductivity field is given by

$$K = \sum_{i=1}^{M} \sum_{k=1}^{M^{(i)}} K^{(i)} I(\mathbf{x} - \mathbf{x}^{(i,k)}) \tag{3.28}$$

where the indicator function I is defined by

$$I(\mathbf{x}-\mathbf{x}^{(i,k)}) = \begin{cases} 1 & \mathbf{x} \in \omega^{(i,k)} \\ 0 & \mathbf{x} \notin \omega^{(i,k)} \end{cases} \tag{3.29}$$

The statistical description of K_i is done by the joint pdf

$$p\left(\mathbf{x}^{(1,1)}, \mathbf{x}^{(1,2)}, ...\right) \tag{3.30}$$

For a flow domain of much larger extension then the block size, tending eventually to infinity, the univariate pdf of $\mathbf{x}^{(i,k)}$ is given by

$$p\left(\mathbf{x}^{(i,k)}\right) = \frac{1}{\Omega} \tag{3.31}$$

The joint pdf $p(\mathbf{x}^{(i,k)}, \mathbf{x}^{(j,t)})$ of two centroids can be derived by using the Bayes relationship

$$p(\mathbf{x}^{(i,k)}, \mathbf{x}^{(j,t)}) = p(\mathbf{x}^{(j,t)}|\mathbf{x}^{(i,k)})p(\mathbf{x}^{(i,k)}) \tag{3.32}$$

where the conditional pdf is

$$p(\mathbf{x}^{(j,t)}|\mathbf{x}^{(i,k)}) = \frac{1}{\Omega - \omega'^{(i,k)}} \tag{3.33}$$

where $\omega'^{(i,k)}$ is the "rejection zone", the portion of the domain where is not possible to find the centroid $\mathbf{x}^{(j,t)}$, standing the non-overlapping constraint. In this case $\omega'^{(i,k)}$ has a shape similar to $\omega^{(i,k)}$ but with dimension twice as $\omega^{(i,k)}$.

The generalization to 3 or more centroids poses geometrical problems when $\overline{\mathbf{x}}^{(j,t)}$ and $\overline{\mathbf{x}}^{(i,k)}$ are closer than 3 semi-axis. For sufficiently distance between $\overline{\mathbf{x}}^{(j,t)}$ and $\overline{\mathbf{x}}^{(i,k)}$ the pdf of the third centroid $\overline{\mathbf{x}}^{(l,s)}$ is

$$p(\overline{\mathbf{x}}^{(l,s)} \, |\overline{\mathbf{x}}^{(j,t)}\overline{\mathbf{x}}^{(i,k)}) = \frac{1}{\Omega - \omega'^{(i,k)} - \omega'^{(j,t)}} \tag{3.34}$$

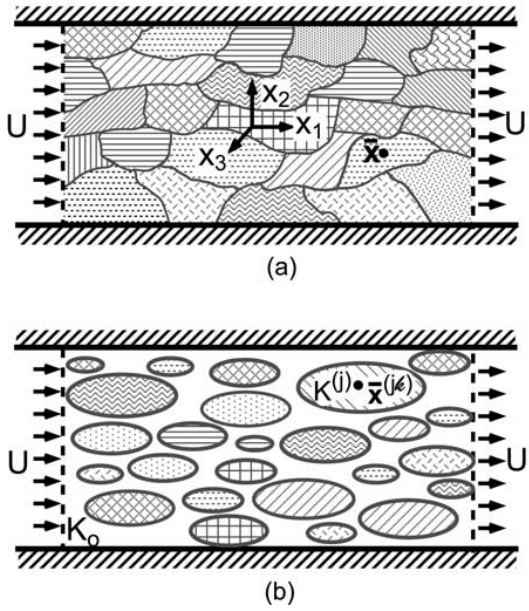

Figure 3.1: Flow domain and boundary conditions: (a) Sketch of a Multi Indicator heterogeneous isotropic structure and (b) model of inclusions of regular shape planted at random in a matrix. From Dagan et al. 2003

To simplify the model a regular shape is assigned to $\omega^{(i,k)}$ (see Fig 3.1), in this case standing the axis-symmetric anisotropy of the natural formations a oblate spheroidal shape is chosen. This shape constitute an idealization of the usual irregular shape of the natural formation. Fixed a cartesian coordinate system the equation of an oblate spheroid characterized by the position centroid $(\overline{x}_1, \overline{x}_2, \overline{x}_3)$ and by the two semi-axes R_h, R_v placed in the space with the major semi-axis alligned with the $x_1$and the x_2 direction is:

$$\frac{(x_1 - x_{1,c})^2 + (x_2 - x_{2,c})^2}{R_h^2} + \frac{(x_3 - x_{3,c})^2}{R_v^2} = 1 \tag{3.35}$$

We call axis ratio $f = R_v/R_h$ and eccentricity $e = \sqrt{(R_h - R_v)/R_h}$.

The inclusions of random hydraulic conductivity K_i are submerged in a matrix of conductivity K_0, hence the hydraulic conductivity field (3.28) is

$$K = \sum_{i=1}^{M} \sum_{k=1}^{M^{(i)}} K^{(i)} I(\mathbf{x} - \mathbf{x}^{(i,k)}) + K_0 \left[1 - \sum_{i=1}^{M} \sum_{k=1}^{M^{(i)}} K^{(i)} I(\mathbf{x} - \mathbf{x}^{(i,k)}) \right] \quad (3.36)$$

If we assume the statistical independence of the centroid positions we have the following relationship for the expected value and for the covariance of the indicator function:

$$\begin{aligned} \left\langle I(\mathbf{x} - \mathbf{x}^{(i,k)}) \right\rangle &= \textstyle\int_\Omega I(\mathbf{x} - \mathbf{x}^{(i,k)}) p(\mathbf{x}^{(i,k)}) d\mathbf{x}^{(i,k)} \\ &= \omega^{(i,k)}/\Omega = n^{(i,k)} \qquad (i,k) \neq (j,t) \\ \left\langle I(\mathbf{x} - \mathbf{x}^{(i,k)}) I(\mathbf{x} - \mathbf{x}^{(j,t)}) \right\rangle &= 0 \qquad (i,k) \neq (j,t) \end{aligned} \quad (3.37)$$

Where $n^{(i,k)}$ is the volume fraction of the inclusion with centroid position $\overline{\mathbf{x}}^{(i,k)}$ and hydraulic conductivity K_i. We define now the volume fraction of the phase K_i, as the summation $n^{(i)} = \sum_{k=1}^{M^{(i)}} n^{(i,k)}$ and the total volume fraction of the inclusions $n = \sum_{i=1}^{M} n^{(i)}$. Finally we can write the mean and the variance of the hydraulic conductivity field

$$\begin{aligned} \langle K \rangle &= \textstyle\sum_{i=1}^{M} K^{(i)} n^{(i)} + K_0(1-n) \\ \sigma_K^2 &= \textstyle\sum_{i=1}^{M} \left(K^{(i)} - \langle K \rangle \right)^2 n^{(i)} + K_0^2(1-n) \end{aligned} \quad (3.38)$$

Taking now the continuous limit for the conductivity K and for the inclusion length scale and we obtain $n^{(i,k)} -> nf(K,R)$ and $n^{(i)} -> nf(K)$ where R is the dimension of he inclusion.

And by the relation (3.36) we obtain the pdf of the conductivity respec-

tively of the medium and of the inclusions

$$\begin{aligned} p_t(K) &= np(K) + (1-n)\,\delta(K-K_0) \\ p(K) &= \textstyle\int p(K,R)dR \end{aligned} \tag{3.39}$$

In the next sections we use the log-permeability $Y = \log(K)$, the previous relations are formally equal.

We derive, for the continuous distribution of Y, the mean and the variace:

$$\begin{aligned} \langle Y \rangle &= n \textstyle\int Y p(Y) + Y_0(1-n) \\ \sigma_Y^2 &= n \textstyle\int \left(Y - \langle Y \rangle\right)^2 p(Y) + (1-n)\left(Y_0 - \langle Y \rangle\right)^2 \end{aligned}$$

The 2-point covariance $C_Y(\mathbf{x}, \mathbf{x}')$ of the generic multi-indicator structure for a dense system ($n = 1$) is

$$C_Y(\mathbf{x},\mathbf{x}') = \sum_{i=1}^{M}\sum_{k=1}^{M^{(i)}}\sum_{j=1}^{M}\sum_{t=1}^{M^{(j)}} \left(Y^{(i)} - \langle Y \rangle\right)\left(Y^{(j)} - \langle Y \rangle\right)\left\langle I(\mathbf{x} - \mathbf{x}^{(i,k)}) I(\mathbf{x}' - \mathbf{x}^{(j,t)})\right\rangle \tag{3.40}$$

Dagan et al. (2003) shows that, for 3-dimensional spheroidal blocks, due to the assumption of lack of correlation between centroids, the contribution pairs of different inclusions to the sum (3.40) tends to 0 as $\omega^{(j,t)}/\Omega - > 0$, hence only the diagonal terms contribute to the (3.40) and the previous relation can be simplified in:

$$\begin{aligned} C_Y(\mathbf{x},\mathbf{x}') = \textstyle\sum_{i=1}^{M}\sum_{k=1}^{M^{(i)}} \left(Y^{(i)} - \langle Y \rangle\right)^2 \left\langle I(\mathbf{x} - \mathbf{x}^{(i,k)}) I(\mathbf{x}' - \mathbf{x}^{(i,k)})\right\rangle = \\ \textstyle\sum_{i=1}^{M}\sum_{k=1}^{M^{(i)}} \left(Y^{(i)} - \langle Y \rangle\right)^2 n^{(i,k)} \chi(r'^{(i,k)}) \end{aligned} \tag{3.41}$$

where

$$\chi(r') = \begin{cases} 1 - \frac{3}{2}r' + \frac{1}{2}r'^3 & r' < 1 \\ \\ 0 & r' > 1 \end{cases} \qquad (3.42)$$

$$r' = \sqrt{\left(x_1^2 + x_2^2\right)/2R_h^2 + \left(x_3\right)^2/2R_v^2}$$

is the *overlap function* defined by the normalized volume of the oblate spheroid overlap ω of semi-axis (R_h, R_h, R_v) and its normalized displacement r. Taking he continuous limit for K and R, and standing the 2-th order stationarity

$$C_Y(\mathbf{r}) = \int\int \left(Y - \langle Y \rangle\right)^2 \chi(r') p(Y, A) dY dR_h \qquad (3.43)$$

The identification of the joint pdf $p(Y, R_h)$ from field data unfortunately is impossible, the only information that can be achieved by expensive field campaign are the mean and correlation structure of the permeability field, and the errors admitted are in practical cases important.

The asymptotic solute spreading in a natural alluvial aquifer is dominated by large scale heterogeneity, in effect for tree dimensional structures Dagan et al. (2003) suggest that alluvial aquifer system may be represented by blocks surrounded by a relatively uniform material. Transport field tests in highly heterogeneous aquifer (Boggs et al. 1992) revealed that the dominating effect upon the solute plume is the presence of low conductivity bocks. We modify consequently the multi indicator structure assuming the simplest model by fixing the dimension of the blocks. This approximation allows important simplifications on the analytical solution. In Fig. 3.2) is shown the simplified MI formation for an isotropic medium.

Summarizing, here, the MI structure is simplified assuming blocks shaped as oblate spheroids, of constant axes and random hydraulic conductivity K_i lognormal distributed. The inclusion are submerged in a uniform matrix

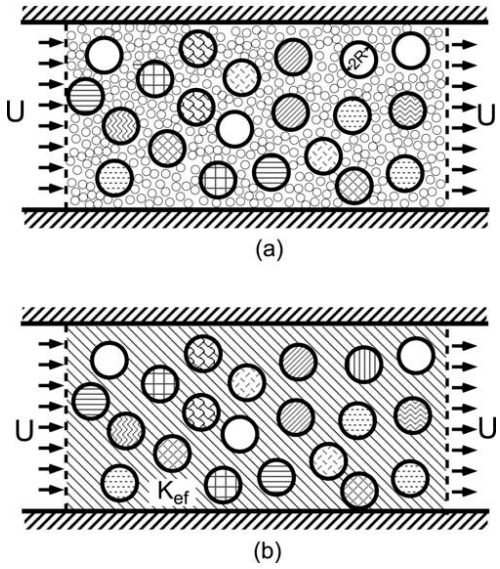

Figure 3.2: An isotropic medium made up from large inclusions (a) surrounded by much smaller ones and (b) by a homogeneous matrix of conductivity K_{ef}. From Dagan et al. 2003

of hydraulic conductivity K_0. The covariance structure of the conductivity reflects the axis-symmetric anisotropy of the medium. The covariance structure in (3.40) can be simplified (Dagan et al., 2003) and assume the following shape:

$$C_Y = \sigma_Y^2 \chi(r') = \begin{cases} \sigma_Y^2(1 - 3r'/2 + r'^3/2) & r' \leq 1 \\ 0 & r' > 1 \end{cases} \quad , \tag{3.44}$$

that is the Semi-spherical covariance structure (see e.g. Dagan, 1989, Rubin, 2003). In Fig. 3.3 is shown the covariance function and the associated semivariogram.

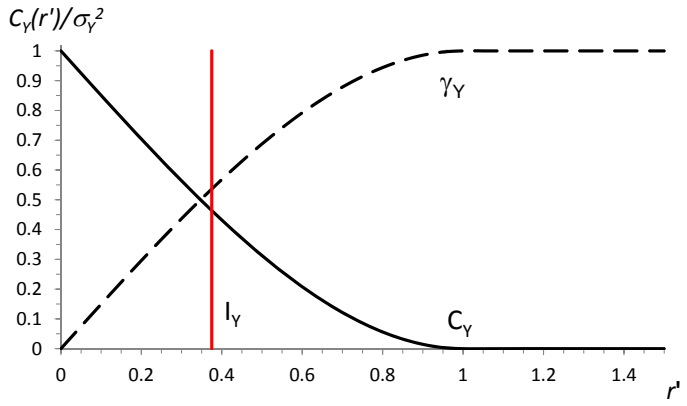

Figure 3.3: Semi-spherical covariance function C_Y and the its associated variogram γ_Y as function of the semi-distance r'

The integral scales in the horizontal and in the vertical directions are

$$\begin{aligned} I_{Yh} = \int_0^\infty \rho_Y(r_1, 0, 0)\, dr_1 = \int_0^\infty \rho_Y(0, r_2, 0)\, dr_2 = \tfrac{3}{4} R_h \\ I_{Yv} = \int_0^\infty \rho_Y(0, 0, r_3)\, dr_3 = \tfrac{3}{4} R_v \end{aligned} \tag{3.45}$$

where $\rho_Y(\mathbf{r}) = C_Y(\mathbf{r})/\sigma_Y^2$ is the autocorrelation function of the log-permeablity Y.

The generalization of the conductivity of the homogeneous matrix surrounding the inclusions is achieved by replacing K_0 by a tensor $\mathbf{K}_0$ of principal axes parallel to $\mathbf{x}$ and of diagonal components K_{0h};K_{0h} and K_{0v}, respectively. The problem of mean uniform flow is stated in this formations as follows:

we denote by $\phi(\mathbf{x}) = -KH/\theta$, the velocity potential, such that by (3.1)

it satisfies the following equations in the domain $\Omega = L_1 L_2 L_3$:

$$\nabla^2\phi(\mathbf{x})=0 \quad (\mathbf{x} \in\Omega) \quad \rightarrow \tag{3.46}$$

$$\rightarrow \begin{cases} \nabla^2\phi^{(in)}=0 & (\mathbf{x} \in\omega) \\ \nabla^2\phi^{(ex)}=0 & (\mathbf{x} \notin\omega) \end{cases} \tag{3.47}$$

by the Darcy law the fluid flux is given

$$\begin{aligned} \mathbf{V}^{(in)} &= -K\nabla\phi^{(in)} \\ \mathbf{V}^{(ex)} &= -\mathbf{K}_0\nabla\phi^{(in)} \end{aligned} \tag{3.48}$$

The boundary conditions are

$$\frac{\partial\phi}{\partial x_1} = U \quad (x_1 = \pm\, L_1/2) \tag{3.49}$$

$$\frac{\partial\phi}{\partial x_i} = 0 \quad (x_i = \pm\, L_i/2)\,, \quad i = 2,3 \tag{3.50}$$

The potential is discontinuous at the interfaces $\partial\omega^{(j)}$ between inclusions and matrix, and the boundary condions at the interfaces are:

$$\frac{\partial\phi_{ex}}{\partial\nu} = \frac{\partial\phi_{in}}{\partial\nu} \tag{3.51}$$

$$\frac{\phi_{ex}}{K_{ef}} = \frac{\phi_{in}}{K^{(i)}} \tag{3.52}$$

where ϕ_{in} is the potential inside the generic inclusion $\omega^{(j)}$, ϕ_{ex} is the exterior one and $\partial/\partial\nu$ is the derivative in the direction ν normal to the spheroidal surface. We take the flow domain dimensions much larger than the spherid semi-axis, respecting the ergodic hypotesis. We represent the potential in a general manner as the summation of the mean potential $\langle\phi\rangle =$

Ux_1 and the potential disturbancies $\varphi^{(i,k)}(\mathbf{x})$ generated in the generic point $\mathbf{x}$ by the inclusion $\omega^{(i,k)}$

$$\phi(\mathbf{x}) = Ux_1 + \sum_{i=1}^{N}\sum_{k=1}^{M^{(i)}} \varphi^{(i,k)}(\mathbf{x}) = Ux_1 + \sum_{j=1}^{N} \varphi^{(j)}(\mathbf{x}) \tag{3.53}$$

where $N = \sum_{i=1}^{M} M^{(i)}$ is the total number of inclusions.

The analytical expression for each potential disturbance $\varphi^{(j)}(\mathbf{x})$ appears as an infinite series, the first term of that series takes into account the effect of the inclusion whose the point x belong, the other terms take into account the effect of the remaining inclusions. coefficients depends in general on the M inclusions constituting the folw domain. The analytical expression for each disturbance appears as an infinite series (Fitts, 1991), efficient numerical procedure to determine the coefficients of these series, in order to satisfy the head matching conditions in (3.1) are described in Jankovic and Barnes (1999), Jankovic et al. (2003). The influence of each inclusion is written as an infinite series, which is truncated in the algorithm implementation. The global flow problem is solved iteratively, by cycling the analysis through all inclusions until differences in the solutions are smaller than a prescribed tolerance. The iterations terminate when the largest relative change of coefficients of the series between two subsequent iterations is less than a prescribed tolerance. Details of the algorithm implementation, which makes use of parallel processing, are given in Suribhatla et al. (2011).

3.3.1 Self-Consistent Approximation

The potential equation in (3.53) does not have a close-form solution. The scope of the present work is to develop approximate, analytical solutions for statistical moments of the velocity field. The approximation we adopt here

known as in the literature as self-consistent or effective medium approximation that was employed for the first time in Dagan 1979 and 1981 in the context of porous formations, and in Dagan et al. (2003) and in Fiori et al. (2003) to study the properties of isotropic media by the MIM.

The kernel of the approximation is to regard the inclusions as non-interacting and submerged in the matrix of conductivity $\mathbf{K}_{ef}$. The value of the hydraulic conductivity of the matrix reflects jointly the presence of neighboring inclusions. The euristic justification of the model is that each inclusion is surrounded by a swarm of inclusions and their non-linear effect is to act as an effective medium (Dagan, 2003). This is similar to a dilute approximation (Eames and Bush, 1999), valid for $n \ll 1$ but with the given matix conductivity $\mathbf{K}_0$ replaced wit the unknown $\mathbf{K}_{ef}$. The use of the effective permeability is necessary to ensure the correct matching with the boundary conditions.

The upscaling of a permeability field with anisotropic covariance structure consit in an anisotropic effective conductivity tensor that reflects the symmetry of the covariace structure, if we define a principal coordinate systems with the principal directions aligned with the principal direction of anisotropy we can write the Hydraulic conductivity tensor as:

$$\begin{pmatrix} K_{efh} & 0 & 0 \\ 0 & K_{efh} & 0 \\ 0 & 0 & K_{efv} \end{pmatrix} \tag{3.54}$$

The potential equation (3.53) is formally the same but the potential disturbancies $\varphi^{(j)}(\mathbf{x})$ in the self-consistent approximation are determined for one single iclusion submerged in a matrix of permeability $\mathbf{K}_{ef}$. This represents a great simplification over the flow problem, as it depends only on the solution φ_j for isolated inclusions, of random K_j and embedded in a homogeneous

matrix of anisotropic conductivity $\mathbf{K}_{ef}$. The solution for φ_j can be obtained from the solution for a spheroid submerged in isotropic conductivity K_{efh} after transformation of the anisotropic background using coordinate scaling

$$\begin{cases} x_s = x_1 \\ y_s = x_2 \\ z_s = \xi x_3 \end{cases} \tag{3.55}$$

$$\begin{cases} \partial x_s = \partial x_1 \\ \partial y_s = \partial x_2 \\ \partial z_s = \xi \partial x_3 \end{cases} \tag{3.56}$$

where $\xi = \sqrt{K_{efh}/K_{efv}}$.

The coordinates (x_s, y_s, z_s) are referred to as scaled cartesian coordinates. Adopting the above transformation in the Laplace equation leads to an isotropic background conductivity, whereas the axis ratio of the spheroids becomes $f_s = f\xi$ and inclusions becomes anisotropic.

The solution for potential disturbance φ for an individual isotropic spheroid of conductivity K submerged in a homogeneous isotropic matrix of conductivity K_{efh} is given in Carslaw and Jaeger (1959), as follows

$$\begin{aligned} \frac{\varphi^{(in)}}{UR} &= -\frac{(\kappa-1)}{1+(\kappa-1)\,A_0\,(f_s)} A_0\,(f_s)\,\frac{r_1}{R} \qquad (\mathbf{r} \in \omega) \\ \frac{\varphi^{(ex)}}{UR} &= -\frac{(\kappa-1)}{1+(\kappa-1)\,A_0\,(f_s)} A_\lambda\,(f_s, \mathbf{r})\,\frac{r_1}{R} \qquad (\mathbf{r} \notin \omega) \end{aligned} \tag{3.57}$$

where

$$A_\lambda = \frac{\sqrt{1-f_s^2}}{2f_s^3}\left(\cot^{-1}\zeta_s\,(\mathbf{r}) - \frac{\zeta_s\,(\mathbf{r})}{\zeta_s^2\,(\mathbf{r})+1}\right) \quad ; \quad A_0 = \frac{\sqrt{1-f_s^2}}{2f_s^3}\left(\cot^{-1}\zeta_0 - \frac{\zeta_0}{\zeta_0^2+1}\right) \tag{3.58}$$

$$\zeta_s\,(\mathbf{r}) = \sqrt{\frac{(Rf_s)^2 + \lambda\,(\mathbf{r})}{R^2\,(1-f_s^2)}} \qquad ; \qquad \zeta_0 = \frac{f_s}{\sqrt{1-f_s^2}}$$

with $\mathbf{r} = \mathbf{x}_s - \overline{\mathbf{x}}$, $r = |\mathbf{r}|$, $\kappa = K/K_{efh}$.

We move now to the velocity field $\mathbf{V}$, which after (3.53) can be written as

$$\mathbf{V}(\mathbf{x}) = \mathbf{U} + \sum_{j=1}^{N} \mathbf{u}_j \left(\mathbf{x}, \bar{\mathbf{x}}_j; K_j\right) \tag{3.59}$$

where $\mathbf{u}_j \left(\mathbf{x}, K_j\right)$ is the velocity disturbance associated with inclusion $\omega^{(j)}$, of conductivity K_j, which is given by $\mathbf{u}_j = \nabla\varphi_j$, the latter being given by (3.57). After (3.57), $\mathbf{u}^{(in)} = \nabla\varphi^{(in)}$ is constant and parallel to the mean flow. Because of the absence of vertical flow inside the spheroid, the solution is also valid for inclusion with anisotropic hydraulic conductivity. $\mathbf{u}^{(ex)}$ depends on the distance between $\mathbf{x}$ and the centroid location $\bar{\mathbf{x}}$, i.e. $\mathbf{u}\left(\mathbf{x}, K\right) = \mathbf{u}\left(\mathbf{x} - \bar{\mathbf{x}}; K\right)$. The derivation of $\mathbf{u}$ and its final expression are given in Appendix A.

The transport analysis requires other approximations and is accurately described in the following chapter 6.

Chapter 4

The Effective Conductivity

The derivation of effective properties of heterogeneous media is one of the central problems of physics and engineering sciences. Replacing the actual medium by an effective, homogeneous one, constitutes the simplest upscaling approach. It is justified when the interest resides in the space average of the variables that characterize the system over scales that are large compared to the heterogeneity scale. Considerable effort has been invested in deriving effective properties for various media and in derivining the range of applicability of the concept. Recent and extensive compendia, in the context of composite materials, are provided by Milton (2002) and Torquato (2002). In this field a comprehensive review has been published by Renard and de Marsily (1997) and Janković et al. (2003); While $K_{ef} = K_G$ was found to be exact for two-dimensional flows no such solution is available in 3D. Though different approximate approaches were forwarded in the past, it is only recently that an accurate numerical solution was derived for highly heterogeneous media. The scope of this section is to test the results obtained by tree different analytical approaches with those obtained through accurate

numerical simulations performed by using the numerical procedure described in Suribhatla et al. 2011, to which the reader is referred to details. The detrmination of the effective hydraulic conductivity for a random medim is based on the first order statistics of the variable charcterizing the flow equations, and formally is:

$$\langle \mathbf{q} \rangle = -\mathbf{K}_{ef} \frac{\partial H}{\partial \mathbf{x}} \tag{4.1}$$

In the following section we recall briefly the method employed to derive the effective property and the study bring on its study.

4.1 First-Order Approximation

In this section we recall briefly the solution developed within first order approximation. The complete solution is fully described in Dagan 1989, Rubin 2003. The strategy is based on eq (3.6). After few passages (see Dagan, 1989 for deatails), the final results for the componets of the effective hydraulic conductivity tensor ($K_{efh}, K_{efh}, K_{efv}$) are:

$$\frac{K_{efh}}{K_G} = 1 + \sigma_Y^2 (\frac{1}{2} - \frac{\lambda}{2}) \tag{4.2}$$

$$\frac{K_{efh}}{K_G} = 1 + \sigma_Y^2 (\frac{1}{2} - \frac{\lambda}{2}) \tag{4.3}$$

where

$$\lambda = \frac{f^2}{1-f^2} (\frac{1}{f\sqrt{1-f^2}} \tan^{-1} \sqrt{\frac{1}{f^2} - 1} - 1) \tag{4.4}$$

and $f = I_{Yh}/I_{Yv}$ is the anisotropy ratio.

It is interesting to note that at first order:

$\mathbf{K}_{ef}$ does not depend on the covariace structure but only on σ_Y^2 and I_{Yh}/I_{Yv};

$\mathbf{K}_{ef}$ reflects the geometric form of the covariance structure, the principal directions of the tensor are parallel to those of the covariace matrix.

4.2 Landau-Matheron's Conjecture

Landau and Lifshitz, for the electodynamic equation, and Matheron, for uniform flow in isotropic and stationary porous media, propose to extend the exact result, in two dimension, to D dimensional space. In 3D and for a lognormal hydraulic conductivity distribution, for isotropic media the relation is

$$\frac{K_{efh}}{K_G} = \exp\left(\sigma_Y^2(\frac{1}{2} - \frac{\lambda}{2})\right) \tag{4.5}$$

This relation examined with the method of perturbation, assuming small the hydraulic conductivity variance σ_Y^2, becomes

$$\frac{K_{efh}}{K_G} = 1 + \sigma_Y^2(\frac{1}{2} - \frac{\lambda}{2}) \tag{4.6}$$

Eq (4.6) is equal to the relation (4.2) obtained by the first-order approximation. We should note that Landau-Matheron conjecture is based on the idea that previous equation (4.2) is the first order expansion of the (4.5). The extension of the (4.5) at anisotropic domains is expressed by relations (see Rubin, 2003 for details)

$$\begin{array}{c} \frac{K_{efh}}{K_G} = \exp\left(\sigma_Y^2(\frac{1}{2} - \frac{\lambda}{2})\right) \\ \frac{K_{efv}}{K_G} = \exp\left(\sigma_Y^2(\frac{1}{2} - (1-\lambda))\right) \end{array} \tag{4.7}$$

where λ is in eq (4.4). Relations (4.7), as the first-order relation do not depend on the covariance structure. Many anthors found that this relations

provide a good fitting of the effective conductivity for an anisotropic domain with lognormal K and exponential covariance (Renard and de Marsily, 1997).

4.3 Self-Consistent Approximation

The application of the self-consistent model to isotropic media is well documented (Dagan, 1979, 1981 and 1989, Janković et al. 2003), it has been applied apparently for the first time to an anisotropic medium of a lognormal $p(K)$ by Dagan (1989, section 3.4.3). For the sake of completeness a simplified derivation is here presented. The analytical solution of this problem is a particular case of the general one discussed in Section 2. Its implementation was carried out in an approximate manner by determining first the head and flux (or velocity) fields by the diluite medim approach. Diluite medim approach consists in neglecting the high-order interactions between inclusions, it is valid for an inclusions fraction $n \ll 1$. Let

$$\mathbf{u}(\mathbf{x}) = \mathbf{V}(\mathbf{x}) - \mathbf{U} \tag{4.8}$$

be the velocity disturbance, defined in $\mathbf{x}$ as the difference between the velocity and the mean velocity. We define the space averaged flux disturbance associated with an isolated inclusions of permeability K surounded by a matrix of tensiorial conductivity $\mathbf{K}_0$ as:

$$\mathbf{u}(K, \mathbf{K}_0) = \int_{\Omega} (\mathbf{V}(\mathbf{x}) - \mathbf{U})\, d\mathbf{x} = \int_{\Omega} \mathbf{u}(\mathbf{x}) d\mathbf{x} \tag{4.9}$$

where Ω is the entire domain. Hydraulic conductivity K is a random function, hence $\mathbf{u}(K, \mathbf{K}_0)$ is random, we can take the ensemble average of the flux as

$$\begin{aligned} \mathbf{U}(\mathbf{K}_0/K_G) &= \int \mathbf{V}(K, \mathbf{K}_0) p(K) dK \\ &= \mathbf{U} + n \int \mathbf{u}(K, \mathbf{K}_0) p(K) dK \end{aligned} \tag{4.10}$$

where $\mathbf{U}$ is the velocity applyed as boundary condition, $n = const$ is the volume fraction of the inclusion, $p(K)$ is the pdf of K. The self-consistent approximation $\mathbf{K}_{sc}$ is obtained from the requirement

$$\mathbf{U}(\mathbf{K}_{ef}/K_G) = \mathbf{U}_\infty \tag{4.11}$$

hence

$$\int \mathbf{u}(K, \mathbf{K}_{sc}) p(K) dK = 0 \tag{4.12}$$

The starting point is the solution of the flow problem in a unbounded domain of conductivity $\mathbf{K}_0(K_{0h}, K_{0h}, K_{0,v})$ surrounding a spheroidal inclusion of conductivity K whose envelope $\partial\omega$ has the equation $(x_1^2 + x_2^2)/R_h^2 + x_3^2/(fR_h)^2 = 1$. Starting with the boundary condition of horizontal flow at infinity $\mathbf{U}(U_\infty, 0, 0)$, in order to apply the self-consistent condition (4.12) we have to integrate $\mathbf{u}(\mathbf{x})$ over the entire domain. However, as it can be found from the general expression of the exterior head field (3.57), and similarly to the spherical inclusions (Janković et al., 2003) the integral of $\mathbf{u}^{(ex)}(\mathbf{x})$ over the space external to the inclusion ω is equal to zero an the only contribution stems from $\mathbf{u}^{(in)}(u^{(in)}, 0, 0)$. Sustituing eq (A.5) in eq (4.12) we obtain the final relation

$$\int_0^\infty \frac{k_h - 1}{1 + (k_h - 1)A_0(f_s)} p(K) dK$$

A similar computation can be carried out for flow at infinity parallel to the z axis, generated by a BC $\mathbf{U} = (0, 0, U_\infty)$. The pertinent coordinate trasformation is

$$\begin{cases} x_u = \xi^{-1} x_1 \\ y_u = \xi^{-1} x_2 \\ z_u = x_3 \end{cases} \tag{4.13}$$

reducing the problem to one of flow in a matrix of conductivity K_{0v} surrounding an inclusion of conductivity K and envelope $\partial\omega_u$, an oblate spheroid of

axis-ratio f_s. The solution (Carslaw and Jaeger, 1959, eq 16.4.10) for the interior velocity field is now

$$\frac{V_z^{(in)}}{U} = \frac{k_v}{1 + (k_v - 1)(1 - 2A_0(f_s))} \tag{4.14}$$

the velocity disturbance is:

$$\frac{u_z^{(in)}}{U_\infty} = \frac{V_z^{(in)}}{U_\infty} - 1 = -\frac{2(k_v - 1)A_0(f_s)}{1 + 2A_0(f_s)(1 - k_v)} \tag{4.15}$$

with $k_v = K/K_{efv}$. Substituing (4.15) in (4.12) we arrive at the final system of equations

$$\begin{cases} \int_0^\infty \frac{k_h - 1}{1 + (k_h - 1)A_0(f_s)} p(K) dK \\ \int_0^\infty \frac{k_v - 1}{k_v + (1 - k_v)2A_0(f_s)} p(K) dK \end{cases} \tag{4.16}$$

with $f_s = f(K_{efh}/K_{efv})^{1/2}$, $k_h = K/K_{efh}$, $k_v = K/K_{efv}$, which is the the final result given in Dagan (1989, eq. 3.4.30 and 3.4.32). Eq (4.16) constitute a system of coupled integrals equations in the unknown K_{efh} and K_{efv} as function of $f = I_v/I_h$, σ_Y^2 ,and the pdf $p(K)$. It can be solved numerically. Under small perturbation expansion $K/K_G = \exp(Y') \simeq 1 + Y' + Y'^2/2$, $\langle Y' \rangle = 0$, $\langle Y'^2 \rangle = \sigma_Y^2$ eqs (4.16) give:

$$\begin{array}{c} \frac{K_{efh}}{K_G} = 1 + \sigma_Y^2(\frac{1}{2} - A_0(f)) \\ \frac{K_{efv}}{K_G} = 1 + \sigma_Y^2(-\frac{1}{2} + 2A_0(f)) \end{array} \tag{4.17}$$

recovering results obtained in the past in the FOA for an arbitrary distribution $p(K)$.

4.4 Results and Discussion

We present here a few results for the horizontal and vertical components of the effective conductivity tensor $\mathbf{K}_{ef}$ obtained by the different analytic methods:

1-the first order approximate solution, eq (4.2)

2-the the exponential conjecture, eq (4.7)

3-the self consistent appriximation, eq (4.16)

These tree methods are tested through a comparison with accurate numerical simulations. We start from analyzing the impact of the inclusions density n, by representing in Figure 4.1 K_{efh}/K_G as function of n for the selected values of the logconductivity variance $\sigma_Y^2 = 2, 4, 8$ (the numerical results are represented by dots). The case examined is $f = 0, 1$, i.e. a strongly anisotropic formation.

Similar to the isotropic case (Janković et al., 2003), the effective conductivity is weakly dependent on n. In other words, if inclusions of a lognormal conductivity distribution are inserted within a large spheroid in a medium of background conductivity $\mathbf{K}_{ef}$, derived by the SC method, the uniform flow outside the spheroid is little disturbed by the presence of the inclusions, irrespective of their density. Since $\mathbf{K}_{sc}$ is derived by assuming the dilute limit $n \to 0$, the weak dependence of $\mathbf{K}_{ef}$ on density is an indirect proof of the validity of the self-consistent solution. As expected, it is seen in Fig. 4.1 that for small values of the density the effective horizontal conductivity is predicted very well by the self consistent solution. It slightly underestimates the effective conductivity for the largest $n = 0.7$, and the discrepancy somewhat increases with the degree of heterogeneity. At any rate, the deviations are very small, considering the high degree of heterogeneity at which they

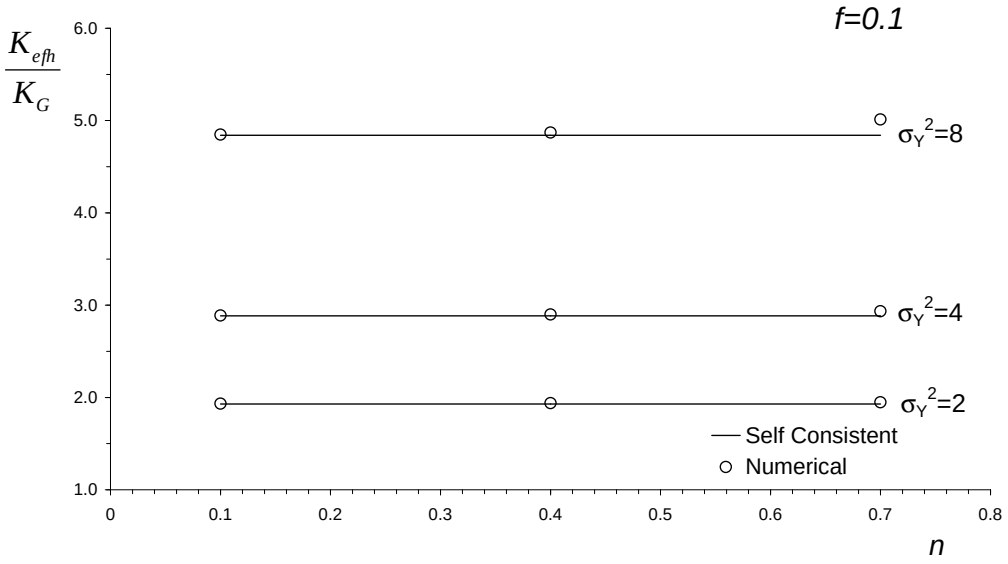

Figure 4.1: The dimensionless horizontal effective conductivity K_{efh}/K_G as function of the inclusions volume density n for a few values of the logconductivity variance σ_Y^2; the anisotropy ratio $f = 0,1$; dots: numerical results; solid lines: self consistent solution.

manifest; similar conclusions can be drawn also for cases of larger anisotropy ratios, which are not represented here for the sake of conciseness.

The behavior of the effective conductivities $K_{efh}; K_{efv}$ as function of σ_Y^2 is illustrated in Figures 4.3, 4.3, 4.4, for different values of the anisotropy ratio f. The self consistent solution (Eq. (4.16), solid lines) is found to be accurate for both components of the effective conductivity tensor, with some small deviations for the largest σ_Y^2, as previously discussed. The first-order solution (Eq. (4.2), dotted lines) is generally close to the numerical simulations, while differences are much larger for the vertical component. Conversely, the exponential conjecture (Eq.(4.7), dash-dotted lines) is generally unable to

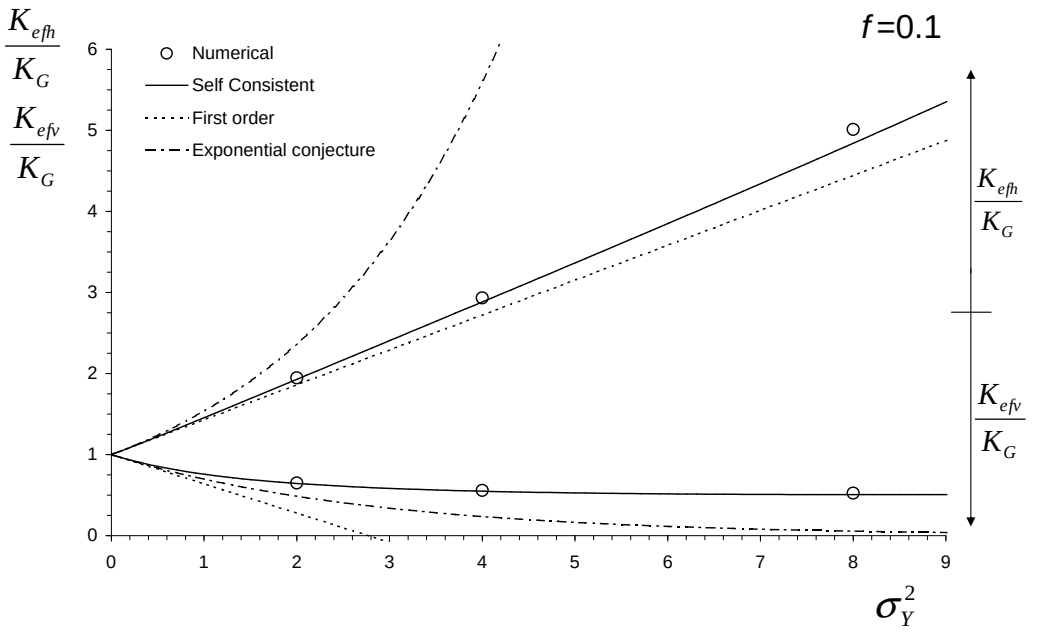

Figure 4.2: The horizontal K_{efh}/K_G and vertical K_{efh}/K_G effective conductivities as function of the logconductivity variance σ_Y^2; dots: numerical results for $n = 0.7$; solid lines: self consistent solution (Eq. 4.16); dotted lines: First order approximation (Eq. 4.2); dot-dashed lines: exponential conjecture (Eq. 4.7); the anisotropy ratio $f = 0.1$.

correctly represent the effective conductivity, especially for high heterogeneity and the horizontal component. Possible reasons for the disagreement are discussed in Janković et al. (2003), the principal one being that the exponential conjecture applicability is dependent on the structure. It is worth noting the nonmonotonous behavior for K_{efv} in the cases $f = 0.2; 0.5$. This behavior cannot be captured by either the first-order solution or its generalization based on the exponential conjecture. The accuracy of the SC model can be explained by the following additional considerations. In all cases,

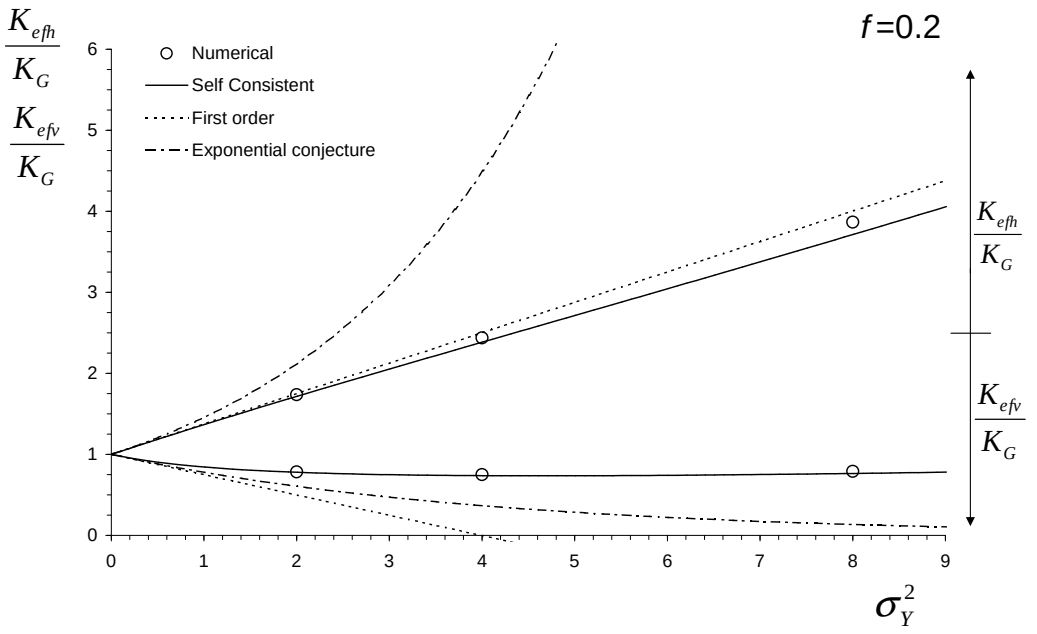

Figure 4.3: The horizontal K_{efh}/K_G and vertical K_{efh}/K_G effective conductivities as function of the logconductivity variance σ_Y^2; dots: numerical results for $n = 0.7$; solid lines: self consistent solution (Eq. 4.16); dotted lines: First order approximation (Eq. 4.2); dot-dashed lines: exponential conjecture (Eq. 4.7); the anisotropy ratio $f = 0.2$

the mean velocity U results from the summation of the interior velocities in the inclusions in all cases. In the dilute approximation, the interior velocity depends only on the conductivity of the inclusion.

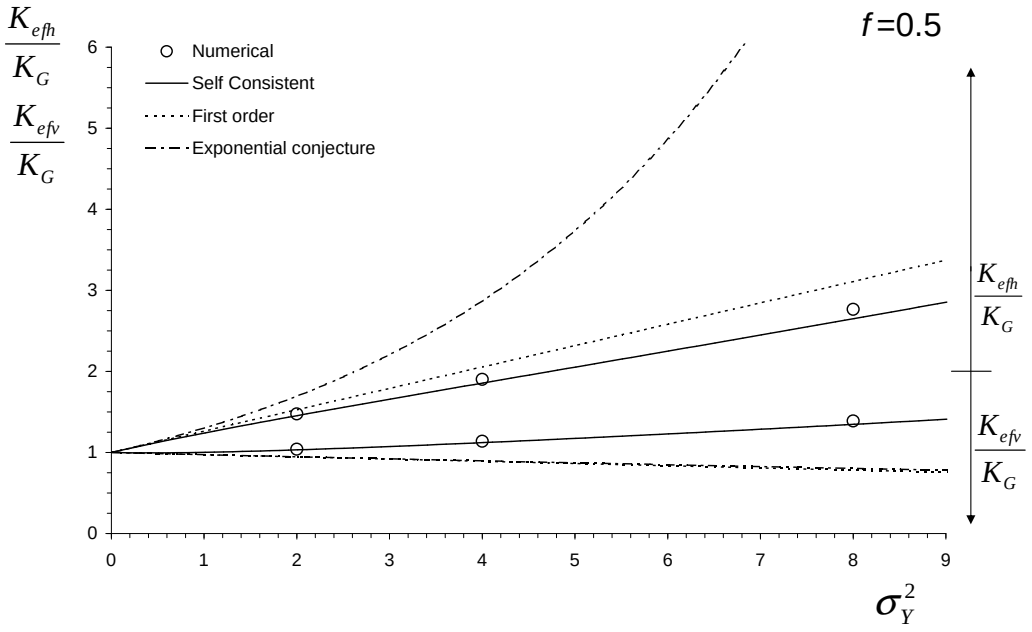

Figure 4.4: The horizontal K_{efh}/K_G and vertical K_{efh}/K_G effective conductivities as function of the logconductivity variance σ_Y^2; dots: numerical results for $n = 0.7$; solid lines: self consistent solution (Eq. 4.16); dotted lines: First order approximation (Eq. 4.2); dot-dashed lines: exponential conjecture (Eq. 4.7); the anisotropy ratio $f = 0.5$

.

Chapter 5

Flow Velocity Statistics for Uniform Flow

The analysis of the velocity statistics in heterogeneous porous formations under mean uniform flow has been the subject of several studies in the past. A significant body of work has been produced along first-order approximation, formally valid for $\sigma_Y^2 \ll 1$ (e.g., Rubin and Dagan, 1992; Zhang and Neuman, 1992; Russo, 1995; Hsu et al., 1996; Russo, 1998), including extensions to higher order corrections, along the same perturbation method (Hsu and Neuman, 1997; Deng and Cushman, 1998). First-order approach has led to a few useful analytical solutions of flow statistics, as function of the structural parameters of the aquifers, such as σ_Y^2, the mean velocity and the anisotropy ratio. However, such solutions suffer from the strong limitation of weak heterogeneity, i.e. they are formally valid for $\sigma_Y^2 \ll 1$. We are not aware of alternative analytical solutions for 3D flows which are free from the above constraint, except those provided by Fiori et al. (2003), which however are derived only for the isotropic formations.

The same problem has been studied through numerical simulations, most of them dealing with isotropic 2D fields (Bellin et al., 1992; Chin and Wang, 1992; Salandin and Fiorotto, 1998; Hassan et al., 1998; Gotovac et al., 2009; de Dreuzy et al., 2007). Extension of the 2D-based results to 3D is not always warranted. A few studies applicable to more realistic 3D anisotropic formations have been conducted in the past (e.g., Burr et al., 1994; Nowak et al., 2008); such investigations are far less numerous than 2D ones. An important problem related to past numerical simulations is that the numerical schemes commonly adopted may not be accurate enough for high values of σ_Y^2 that require extremely fine discretizations and very large domains (Janković et al., 2003; de Dreuzy et al., 2007). An excellent analysis of the velocity statistics in 3D anisotropic fields is provided by Englert et al. (2006), who carry out Monte-Carlo experiments and compare them to analytical solutions of the first- and second-order approximations.

The goal of the present work is to derive analytical solutions for the velocity moments, up to the fourth order, valid for any σ_Y^2. The approach used here is an alternative to the classic first-order perturbation method, and is based on the self-consistent method which was developed in the past for isotropic formations (Dagan et al., 2003; Fiori et al., 2003). The approach is extended here for the first time to the practically relevant case of anisotropic formations with flow parallel to the long axis of anisotropy. This is a non-trivial extension that requires a complete overhaul of all components of the self-consistent methodology. The solutions derived here, although approximate, may be used for preliminary assessments of flow variability whenever flow can be considered locally as uniform in the average, e.g. for slowly varying flow (in space) or regional flow.The approximate solutions shall be compared with the results of the numerical simulations, details of numerical

simulations are in Suribhatla et al. (2011).

5.1 Self-Consistent Approximation

We move now to the velocity field $\mathbf{V}$ in a multi indicator formation, which after applying the self-consistent approximation can be written as

$$\mathbf{V}(\mathbf{x}) = \mathbf{U} + \sum_{j=1}^{N} \mathbf{u}_j \left(\mathbf{x}, \bar{\mathbf{x}}_j; K_j\right) \tag{5.1}$$

where $\mathbf{u}_j \left(\mathbf{x}, \bar{\mathbf{x}}_j; K_j\right)$ is the velocity disturbance associated with inclusion ω_j of conductivity K_j, which is given by $\mathbf{u}_j = \nabla\varphi_j$, the latter being given by (A.5)

After (3.57), $\mathbf{u}^{(in)} = \nabla\varphi^{(in)}$ is constant and parallel to the mean flow. Because of the absence of vertical flow inside the spheroid, the solution is also valid for inclusion with anisotropic hydraulic conductivity. $\mathbf{u}^{(ex)}$ depends on the distance between $\mathbf{x}$ and the centroid location $\bar{\mathbf{x}}$, i.e. $\mathbf{u}\left(\mathbf{x}, \bar{\mathbf{x}}; K\right) = \mathbf{u}\left(\mathbf{x} - \bar{\mathbf{x}}; K\right)$. The derivation of $\mathbf{u}$ and its final expression are given in Appendix A.

The mean velocity is obtained by ensemble averaging of (5.1) over the centroid coordinates $\overline{\mathbf{x}}_j$ and the random conductivity K_j; the corresponding pdf of both variables are denoted as $p\left(\overline{\mathbf{x}}_j\right)$ and $p\left(K_j\right)$, respectively. Since $p(\overline{\mathbf{x}}_j) = 1/\Omega$ (the centroids of the inclusions are generated with uniform probability) and $\mathbf{u}$ depends on $\mathbf{x} - \bar{\mathbf{x}}_j$, this is tantamount to averaging over the space, i.e. integrating over $\mathbf{x}$, while keeping the centroids fixed

$$\begin{aligned} \langle \mathbf{V}(\mathbf{x}) \rangle &= \mathbf{U} + \langle \mathbf{u} \rangle \\ \langle \mathbf{u} \rangle &= \frac{1}{\Omega} \sum_{j=1}^{N} \int_{\Omega} \int \mathbf{u}_j \left(\mathbf{x}; K_j\right) p\left(K_j\right) dK_j d\mathbf{x} \end{aligned} \tag{5.2}$$

The self-consistent or effective medium argument requires that $\langle \mathbf{V} \rangle \equiv \mathbf{U}$. Since in an unbounded domain the contribution of the exterior velocity originating from (3.57) is zero, the condition $\langle \mathbf{V} \rangle \equiv \mathbf{U}$ leads in (5.2) to

$$\begin{array}{c} \langle \mathbf{u} \rangle = \frac{1}{\Omega} \sum_{j=1}^{N} \int_{\Omega} \int \mathbf{u}_j \left(\mathbf{x}; K_j \right) p \left(K_j \right) dK_j d\mathbf{x} = \\ = \frac{1}{\Omega} \sum_{j=1}^{N} \int \mathbf{u}_j^{(in)} \left(K_j \right) \omega_j p \left(K_j \right) dK_j = 0 \end{array} \tag{5.3}$$

where ω_j is the volume of the inclusion and N is the total number of the spheroids in the domain Ω.This condition was used in the previous section in order to derive the value of $\mathbf{K}_{ef}$, and in particular its principal components $K_{efh}, K_{efh}, K_{efv}$;

We derive now the velocity covariance

$$u_{ms} \left(\mathbf{x} - \mathbf{y} \right) = \left\langle \left(V_m \left(\mathbf{x} \right) - U_m \right) \left(V_s \left(\mathbf{y} \right) - U_s \right) \right\rangle \tag{5.4}$$

The latter is derived from (5.1) as follows

$$u_{ms} \left(\mathbf{x} - \mathbf{y} \right) = \left\langle \sum_{j=1}^{N} \sum_{k=1}^{N} u_{j,m} \left(\mathbf{x} - \bar{\mathbf{x}}_j \right) u_{k,s} \left(\mathbf{y} - \bar{\mathbf{x}}_k \right) \right\rangle \quad ; \quad (m, s = 1, 2, 3) \tag{5.5}$$

where $u_{j,m}$ and u_{ks} are respectively the m- and the s-th component of velocity disturbance generated by the j- and the k-th spheroid. Details of the procedure for the averaging of (5.5) are given in Appendix B. It is seen that the off-diagonal terms of the double summation ($i \neq j$) can be neglected: for x fixed in an inclusion of conductivity K, the average of u at a point y outside the inclusion tends to zero by mutual cancelation. Hence, under this approximation only the diagonal terms of the double summation remain in

(5.5). The final result leads to (see Appendix B for details)

$$u_{ms}(\mathbf{x}-\mathbf{y}) = \frac{n}{\omega}\int\int u_m(\mathbf{y}-\mathbf{x}+\overline{\mathbf{x}};K)\,u_s(\overline{\mathbf{x}};K)\,p(K)\;d\overline{\mathbf{x}}\,dK \qquad (m,s=1,2,3) \tag{5.6}$$

The velocity variances $\sigma^2_{mm} = u_{mm}(0)$ are given by

$$\sigma^2_{mm} = \frac{n}{\omega}\int\int u^2_m(\overline{\mathbf{x}};K)\,p(K)\;d\overline{\mathbf{x}}\,dK \qquad (m=1,2,3) \tag{5.7}$$

Inspection of the expressions for $\mathbf{u}$ (eqs. 3.57) reveals that the velocity can be written as the product of two functions, one depending on the conductivity K and the other on the spatial coordinates. Consequently, substitution in (5.6) allows for separate integration over space and K, leading to the following formula

$$u_{mm}(\mathbf{x}-\mathbf{y}) = \sigma^2_{mm}\rho_{mm}(\mathbf{y}-\mathbf{x}) \qquad (m=1,2,3) \tag{5.8}$$

where $\rho_{m\mathbf{m}}(\mathbf{y}-\mathbf{x})$ are the velocity autocorrelation functions, which depend only on the inclusions arrangement and the anisotropy ratio. Hence, the velocity autocorrelation function does not depend on the heterogeneity of hydraulic conductivity, and it is the same as the one obtained by first-order stochastic models, although with a scaled anisotropy ratio $f_s = \xi f$; it is reminded here that $\rho_{22}(x_1)$ and $\rho_{33}(x_1)$ are both hole-type covariances, i.e. with zero horizontal integral scale (see, e.g., Rubin, 2003). Calculation of ρ_{mm} through the first-order analysis is more convenient than performing a multiple integration along (5.6), and we shall follow that procedure, which is well known and documented (see, e.g., Rubin, 2003); The method is fully described in the next paragraph.

With a procedure similar to that leading to (5.7) we analyze the third

and fourth moments of velocity using the following general expression

$$\mu_{i,m} = \left\langle \left(V_m\left(\mathbf{x}\right) - U_m\right)^i \right\rangle = \frac{n}{\omega} \int \int u_m^i(\overline{\mathbf{x}}; K)\, p(K)\; d\overline{\mathbf{x}}\, dK \quad (m = 1, 2, 3) \tag{5.9}$$

with $\mu_{i,m}$ being the i-order central moment of velocity u_m, for example $\mu_{2,m} = \sigma^2_{mm}$. For the latter, it is convenient to recast the problem in spheroidal coordinates, as outlined in the Appendix A.

A close form for the analytical solution of the i-order moment $\mu_{i,m}$ of velocity u_m (Eq. 5.9) was not found and we derive the quantities by numerical quadratures. These are performed by splitting the integrals in two contributions, pertaining to interior and exterior flow, as follows

$$\mu_{i,m} = \mu_{i,m}^{(in)} + \mu_{i,m}^{(ex)} \quad (m = 1, 2, 3) \tag{5.10}$$

with

$$\mu_{i,m}^{(in)} = \int_0^{+\infty} \left(u_m^{(in)}\right)^i p\left(k\right) d\kappa \tag{5.11}$$

$$\begin{gathered} \mu_{i,m}^{(ex)} = \tfrac{1}{\omega} \int_{\zeta_0}^{+\infty} \int_{-1}^{+1} \int_{-\pi}^{\pi} \int_0^{+\infty} \left(u_m^{(ex)}\right)^i \left(\zeta_s^2 + \eta_s^2\right) R^3 * \\ \left(1 + f_s^2\right)^{3/2} p\left(k\right) d\zeta_s d\eta_s d\psi_s dk \quad (m = 1, 2) \end{gathered} \tag{5.12}$$

$$\begin{gathered} \mu_{i,m}^{(ex)} = \tfrac{1}{\omega} \tfrac{1}{\xi^i} \int_{\zeta_0}^{+\infty} \int_{-1}^{+1} \int_{-\pi}^{\pi} \int_0^{+\infty} \left(u_m^{(ex)}\right)^i \left(\zeta_s^2 + \eta_s^2\right) R^3 * \\ \left(1 + f_s^2\right)^{3/2} p\left(k\right) d\zeta_s d\eta_s d\psi_s dk \quad (m = 3) \end{gathered} \tag{5.13}$$

where we have employed the volume scale factor for spheroidal coordinates $dx_s dy_s dz_s = R^3 \left(1 - f_s^2\right)^{3/2} \left(\zeta_s^2 + \eta_s^2\right) d\zeta_s d\eta_s d\psi_s$.

5.2 First-Order Approximation

Under the First-Order assumption the pdf of the velocity is Gaussian for any value of the log-conductivity variance. In fact if the log-conductivity

Y is normally distributed the same is for the velocity V because the linear relationship between Y and V. The expressions of the Fourier Transform (FT) of the velocity covariance under the first-order approximation are given by (see, e.g., Dagan; 1989; Gelhar, 1993; Rubin, 2003)

$$\begin{aligned} \widehat{u}_{ii}(\mathbf{k}) &= \tfrac{1}{(2\pi)^{3/2}} \int_{-\infty}^{+\infty} u_{ii}(\mathbf{x}) \exp(-i\mathbf{x}\cdot\mathbf{k}) d\mathbf{x} = \\ &= U^2 \left[\delta_{1,i} - \tfrac{k_1 k_i}{k^2}\right]^2 \widehat{C}_Y(\mathbf{k}) \end{aligned} \tag{5.14}$$

where $\mathbf{k} = (k_1, k_2, k_3)$ and $\widehat{C}_Y(\mathbf{k})$ is the FT of the logconductivity covariance; the latter is given by (Fiori et al., in press)

$$\begin{aligned} \widehat{C}_Y(\mathbf{k}) &= \tfrac{1}{(2\pi)^{3/2}} \int_{-\infty}^{+\infty} C_Y(\mathbf{x}) \exp(-i\mathbf{x}\cdot\mathbf{k}) d\mathbf{x} = \\ &3\sqrt{\tfrac{2}{\pi}} f \sigma_Y^2 \tfrac{[\sin(Rk_s) - Rk_s\cos(Rk_s)]^2}{k_s^6 R^3} \end{aligned} \tag{5.15}$$

with $k_s = \sqrt{k_1^2 + k_2^2 + (fk_3)^2}$.

The variance of the velocity in the i-direction is obtained by inversion of (5.14) for $\mathbf{r} = 0$, and the resulting analytical expressions are given by

$$\begin{aligned} \tfrac{\sigma_{11}^2}{U^2} &= \sigma_Y^2 \tfrac{\sqrt{1-f^2}\left(6f^4-13f^2+16\right)+f\left(4f^2-13\right)\sin^{-1}\sqrt{1-f^2}}{16(1-f^2)^{5/2}} \\ \tfrac{\sigma_{22}^2}{U^2} &= \sigma_Y^2 f \tfrac{f\sqrt{1-f^2}\left(2f^2+1\right)-\left(4f^2-1\right)\sin^{-1}\sqrt{1-f^2}}{16(1-f^2)^{5/2}} \\ \tfrac{\sigma_{33}^2}{U^2} &= \sigma_Y^2 f \tfrac{-3f\sqrt{1-f^2}+\left(2f^2+1\right)\sin^{-1}\sqrt{1-f^2}}{4(1-f^2)^{5/2}} \end{aligned} \tag{5.16}$$

In the (A.2)and (A.3), we showed that the velocity fluctuation in the SC method can be written as a product of two factors: the first is a function of both the hydraulic conductivity k and the anisotropy ratio f_s, while the second depends on both the position $\mathbf{x}$ and the anisotropy f_s. Consequently, the theoretical autocorrelation function ρ_{mm} of the velocity equals the one adopted in first-order approximation, provided that the scaled anisotropy f_s is used instead of f .

In the first order approximation, for all the 3 velocity components, the 3-th order moments of the velocity are always null, the 4-th order moments are $3\sigma_{ii}$ $(i = 1, 2, 3)$.

The autocorrelation functions are computed by means of inverse FT of (5.14). To this aim, we employ cylindrical coordinates in the frequency domain $k_1 = \rho\cos\theta, \quad k_2 = \rho\sin\theta, \quad k_3 = k_3$, $dk_1 dk_2 dk_3 = \rho d\rho d\theta dk_3$. The final result is obtained by

$$\rho_{mm}(x_j) = \frac{1}{\sigma_{mm}^2}\frac{1}{\sqrt{(2\pi)^3}}\int_0^{+\infty}\int_0^{2\pi}\int_{-\infty}^{+\infty}\widehat{u}_{mm}\cos(k_j x_j)\,\rho d\rho d\theta dk_3 \;;\; j = 1,2 \tag{5.17}$$

$$\rho_{mm}(x_3/\xi) = \frac{1}{\sigma_{mm}^2}\frac{1}{\sqrt{(2\pi)^3}}\int_0^{+\infty}\int_0^{2\pi}\int_{-\infty}^{+\infty}\widehat{u}_{mm}\cos(k_3 x_3/\xi)\,\rho d\rho d\theta dk_3$$

While analytical integration over θ is possible (the result is not given here), numerical quadratures over $\rho,\ k_3$ are needed.

The velocity integral scales I_{u_m} are evaluated from the well known first-order expression $\sigma_Y^2 I_Y = \sigma_{mm}^2 I_{u_m}$, which leads to

$$I_{u_m}\left(f, \sigma_Y^2\right) = \frac{\sigma_Y^2 I_Y}{\sigma_{mm}^2(f_s)} m = 1, 2, 3 \tag{5.18}$$

5.3 Results and Discussion

We present here a few results for the velocity statistical moments obtained by the self-consistent approach described above. The results shall be compared with those obtained by fully numerical simulations which are free from the model approximations and with those obtained from first-order analysis formally valid for $\sigma_Y^2 \ll 1$ (see, e.g., Dagan, 1989; Rubin, 2003). The numerical procedure employed is that developed by Suribhatla et al. (2011) that solves the multi-indicator structure without SC approximation. The statistical quantities, evaluated for normally distributed $Y = \ln K$ normal, are compared with numerical simulations for the following combination of parameters: $\sigma_Y^2 = 2, 4, 8$ and $f = 0.1, 0.2, 0.5$; the isotropic case ($f = 1$) has been analyzed elsewhere (Janković, 2003) and will not be further discussed here. The volume fraction is set to the values $n = 0.1, 0.4, 0.7$, the latter being close to the maximum density achievable by the present setup. We examine first the longitudinal velocity variance σ_{11}^2 (Eq. 5.7) as function of the logconductivity variance σ_Y^2. The main results are displayed in Fig. (5.1) (solid lines), for three values of the anisotropy ratio f. First-order (dashed line, Eq. 5.16) and numerical results (dots) are also displayed. Similar to what was found for the isotropic case (Fiori et al. 2003), the variance grows less than linearly with σ_Y^2. The rate of growth increases with increasing anisotropy. For low density, $n = 0.1$, the SC solution approximates very well the exact one (dots); this is not surprising as the SC solution is based on the dilute approximation, which is formally valid for $n \ll 1$. The SC solution deteriorates with increasing density and heterogeneity, as the nonlinear interactions (neglected in the SC approach) between the inclusions become stronger. Still, the predictions made by First-order analysis (see dashed

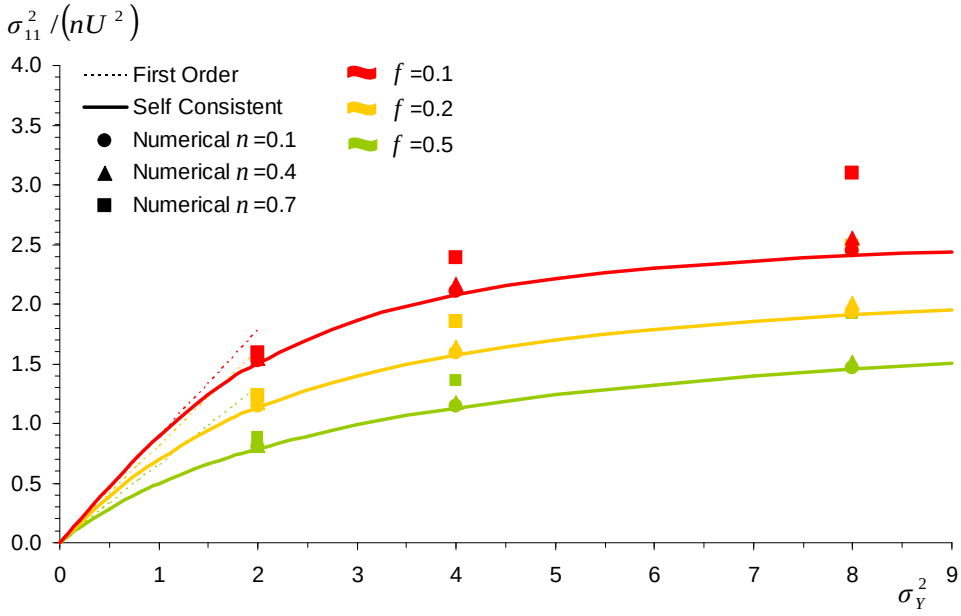

Figure 5.1: Longitudinal velocity variance σ_{11}^2 as function of the logconductivity variance σ_Y^2, for $f = 0.1, 0.2, 0.5$. Self-consistent (solid lines), Numerical Simulations (dots) and First-Order (dashed lines) results.

lines), which typically overpredict the variance when $\sigma_Y^2 \geq 1$.

Similar considerations can be drawn for the variance of the transverse (σ_{22}^2, Fig. 5.2) and vertical (σ_{33}^2, Fig. 5.3) components of the velocity. For such cases the growth of the variance with σ_Y^2 is now inversely proportional to the anisotropy ratio f. The trends are similar to those predicted by First-order analysis (dashed lines), although the latter provides an adequate representation only for relatively low heterogeneity. For very dense systems ($n = 0.7$) the nonlinear interactions are much stronger than for the longitudinal case (see Janković et al., 2003 and Suribhatla et al., 2011), leading to a considerable increase of the transverse and vertical velocity fluctuations with

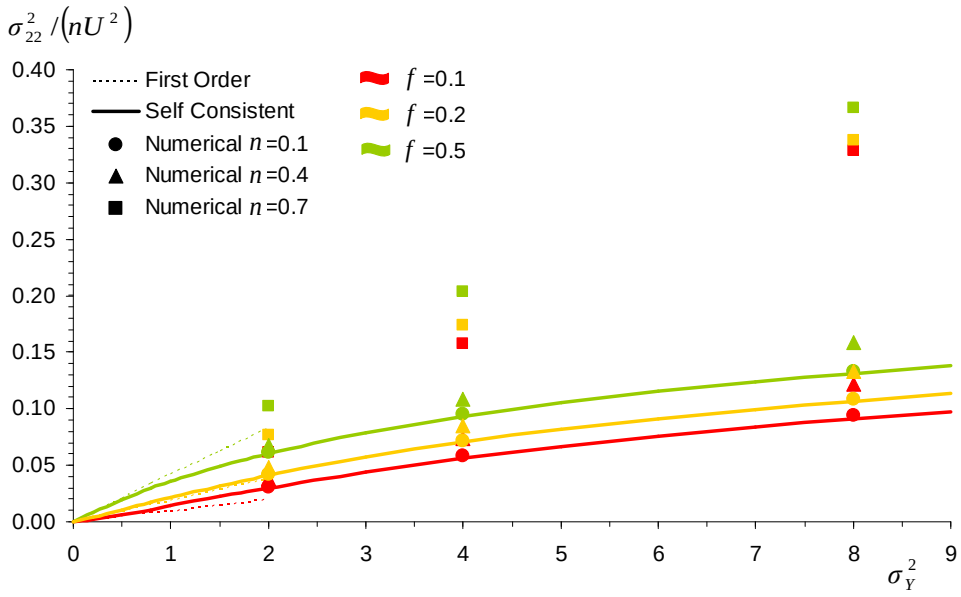

Figure 5.2: Transverse velocity variance σ_{11}^2 as function of the logconductivity variance σ_Y^2, for $f = 0.1, 0.2, 0.5$. Self-Consistent (solid lines), Numerical Simulations (dots) and First-Order (dashed lines) results.

increasing density. Thus, the SC solution provides a reasonable estimate for the variance when $n \simeq 0.4$. Quite interestingly, σ_{33}^2 (σ_Y^2) exhibits a nonmonotonic behavior for high anisotropy (see Fig. 5.3); this is due to the increase of K_{efh} with anisotropy and heterogeneity, leading to a stronger preferential horizontal flow as compared to vertical.

The velocity skewness $sk_{mm} = \mu_{3,m}/\sigma_{mm}^{3/2}$ is depicted in Figure 5.4 for the longitudinal component $m = 1$. While the skewness of the transverse and vertical velocities (not shown in the Fig. 5.4) are always null the skewness of V_1 is significant, and it strongly depends on the degree of heterogeneity and anisotropy, as shown in Figure 5.4. The skewness is close to zero only

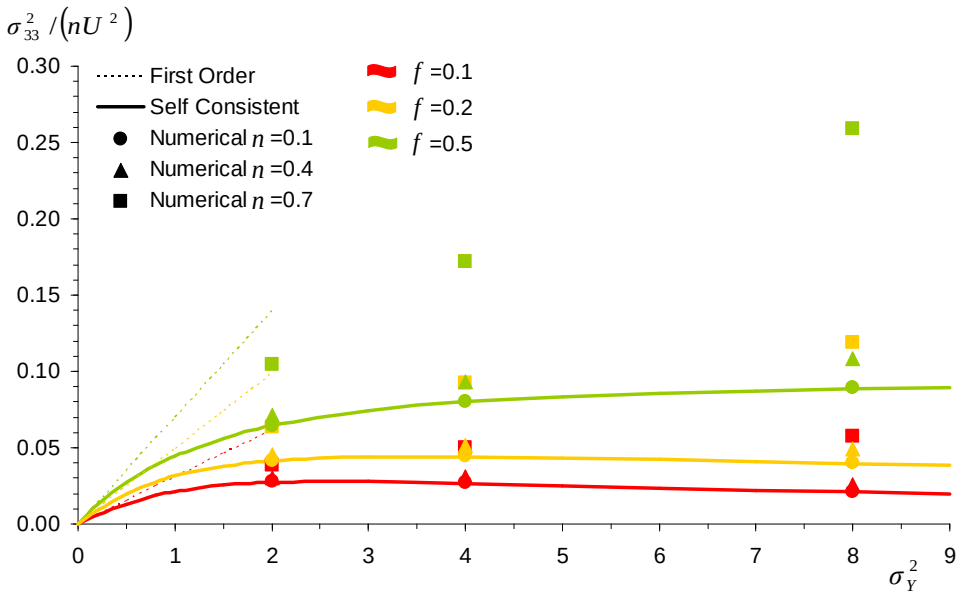

Figure 5.3: Vertical velocity variance σ_{11}^2 as function of the logconductivity variance σ_Y^2, for $f = 0.1, 0.2, 0.5$. Self-Consistent (solid lines), Numerical Simulations (dots) and First-Order (dashed lines) results.

for very small σ_Y^2, for which the velocity pdf is nearly Gaussian. It increases with heterogeneity in a nonmonotonous way, displaying a maximum around $\sigma_Y^2 \cong 2$. Anisotropy generally leads to a larger skewness, hence to a more asymmetrical longitudinal velocity pdf. The skewness is well captured by the SC model for low density, say $n \simeq 0.4$, and the prediction deteriorates with increasing density, consistent with the other statistical quantities examined above.

The picture is similar for the kurtosis $ku_{11} = \mu_{4,1}/\sigma_{11}^2$ (Fig. 5.5), for which the predictions made by the SC model for the highest density $n = 0.7$ are worse than those for the lower statistical moments. This was expected,

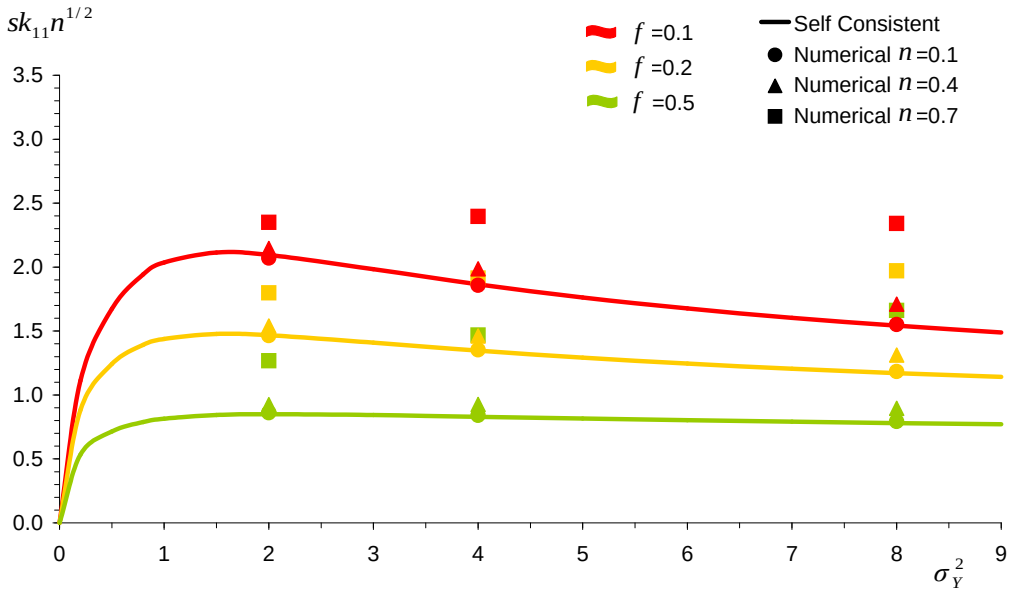

Figure 5.4: Skewness of the longitudinal velocity as function of the logconductivity variance σ_Y^2, for $f = 0.1, 0.2, 0.5$. Self-Consistent (solid lines) and Numerical Simulations (dots).

as the effect of the nonlinear interactions between inclusions becomes more important with increasing order of the statistical moments. The kurtosis is generally far from the Gaussian value $ku_{11} = 3$, except for extremely low heterogeneity. This confirms that the longitudinal velocity for anisotropic heterogeneous systems is generally non-Gaussian, even for low levels of heterogeneity. Results are similar for the vertical and transverse components (not shown), although the kurtosis is generally smaller for those cases. A similar behavior was observed by Nowak et al. (2008), who found an empirically good fit between the components of the specific discharge and the exponential power distribution.

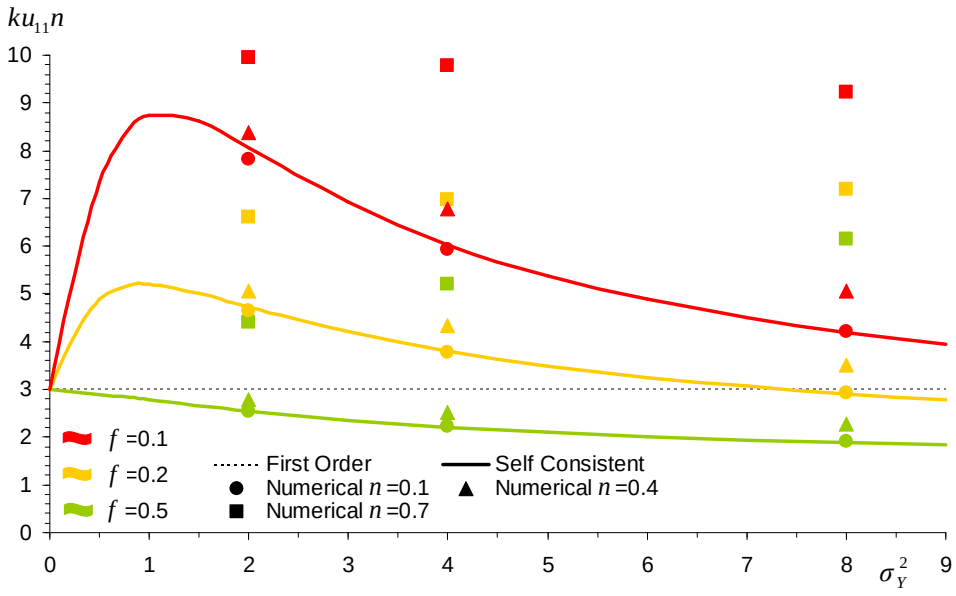

Figure 5.5: Kurtosis of the longitudinal velocity as function of the logconductivity variance σ_Y^2, for $f = 0.1, 0.2, 0.5$. Self-Consistent (solid lines), Numerical Simulations (dots) and First-Order (dashed lines).

Next we examine the velocity autocorrelation function $\rho_{mm}(r_s)$; of particular interest, in view of the analysis of solute transport (not performed here), is the behaviour along the longitudinal direction r_1, as $\rho_{mm}(r_1)$ closely reflects macrodispersivity for low/mild heterogeneity (see the classic developments of the first-order-analysis, e.g., Rubin, 2003). The SC model developed here predicts that ρ_{mm} is not affected by heterogeneity. We check this finding in Figure 5.6, which represents the analytical and the numerically-obtained $\rho_{11}(r_1)$ for a few logconductivity variances σ_Y^2 and anisotropy ratios $f = 0.1, 0.5$; the density is in all cases set to the maximum $n = 0.7$. Inspection of Figure 5.6 confirms that the autocorrelation function ρ_{11} is almost

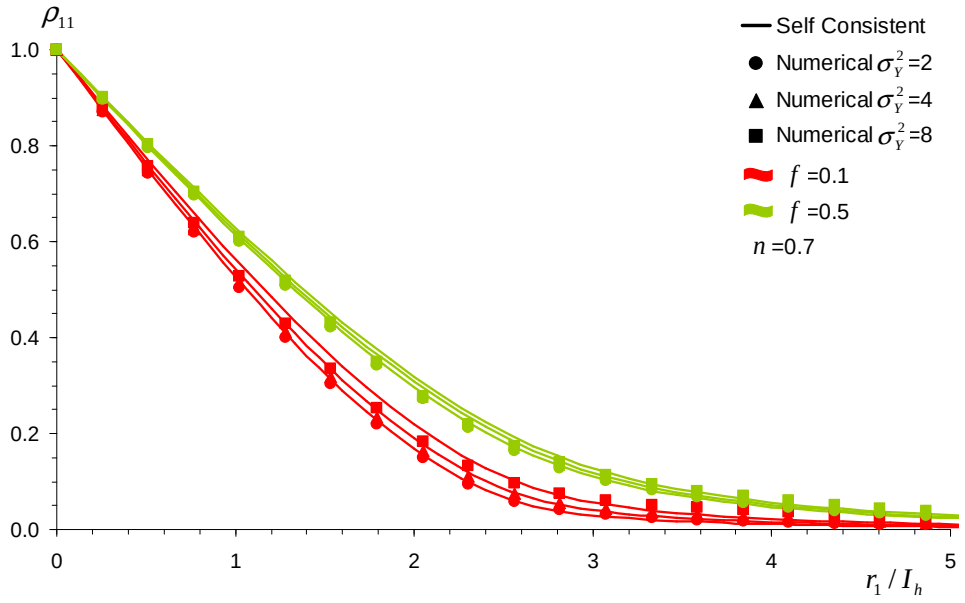

Figure 5.6: Autocorrelation function of the longitudinal velocity (ρ_{11}) as function of longitudinal distance x_1, for $f = 0.1, 0.5$, $\sigma_Y^2 = 2, 4, 8$ and $n = 0.7$; Self-Consistent (solid lines) and Numerical Simulations (dots).

independent on σ_Y^2; the same is found for the other velocity components (not shown in the Figure).

We represent in Figure 5.7 $\rho_{11}(r_1)$ and $\rho_{22}(r_1)$ for a few values of n and for $f = 0.1$ (Fig. 5.7a) and $f = 0.5$ (Fig. 5.7b); standing the weak dependence on σ_Y^2,we shall focus for brevity on the largest variance examined $\sigma_Y^2 = 8$. Comparison between the SC solution (solid line) and numerical simulations (dots) show that $\rho_{11}(r_1)$ is always well represented by the SC solution (solid line). The effects of the nonlinear interactions, which increase with the density n, are not significant for the longitudinal velocity. Anisotropy leads to a general increase of the correlation; this point shall be retaken later. The

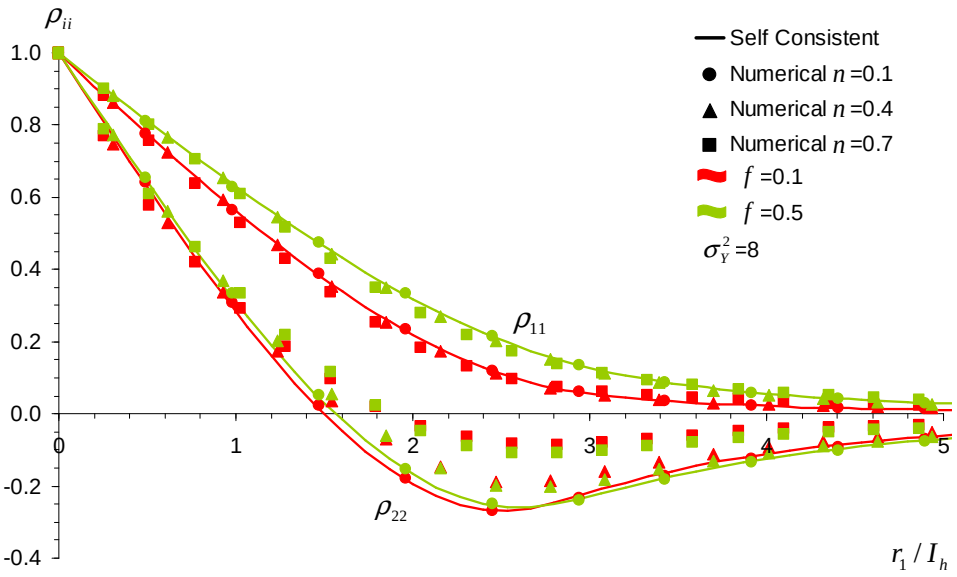

Figure 5.7: Autocorrelation function of the longitudinal (ρ_{11}) and lateral (ρ_{22}) velocities as function of longitudinal distance x_1, for $f = 0.1$ (a), $f = 0.5$ (b); $n = 0.1, 0.4, 0.7$ and $\sigma_Y^2 = 8$; Self-Consistent (solid lines) and Numerical Simulations (dots).

transverse autocorrelation ρ_{22} is also well represented by SC for the lower densities; however, the inclusions interactions play a more important role in increasing the correlation in the negative part, and as a consequence ρ_{22} is no longer a hole- type covariance. The situation is nearly identical for the vertical component ρ_{33} (not shown in the Figure), with values very similar to ρ_{22}.

The other components of the velocity autocorrelation function are also predicted rather well by the SC method. As an example, we represent in Figure 5.7b the behavior of ρ_{11} along the transverse x_2 and vertical x_3 direc-

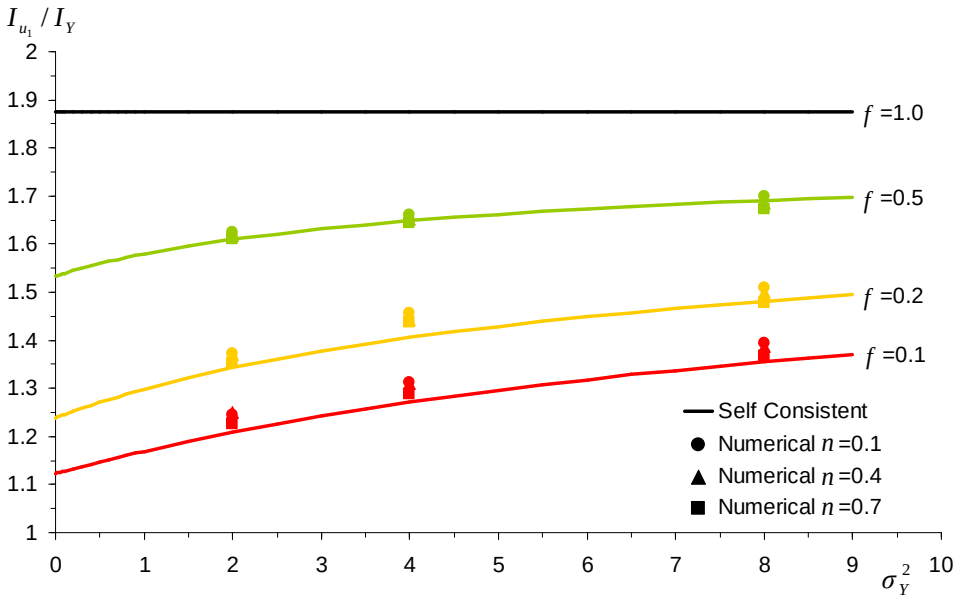

Figure 5.8: Longitudinal integral scale of longitudinal velocity (I_{u_1}), as function of the logconductivity variance σ_Y^2, for a few values of the anisotropy ratio f and the density n. Self-Consistent (solid lines) and Numerical Simulations (dots).

tions for $\sigma_Y^2 = 8,\ f = 0.1$. The validity of SC predictions is similar for other components, and they will not be further discussed here.

The longitudinal integral scale $I_{u_m} = \int_0^\infty \rho_{mm}(r_1)\, dr_1$ is a synthetic measure of the degree of correlation of velocity along the mean flow direction, and it nicely summarizes the above results. Along the first-order stochastic theory, I_{u_m} is proportional to the m component of the macrodispersion tensor. SC-based integral scales are represented in Figures 5.8, together with the numerical results. The good agreement between the numerical results and the SC prediction for I_{u_1} (Figure 5.8) is not surprising, considering the

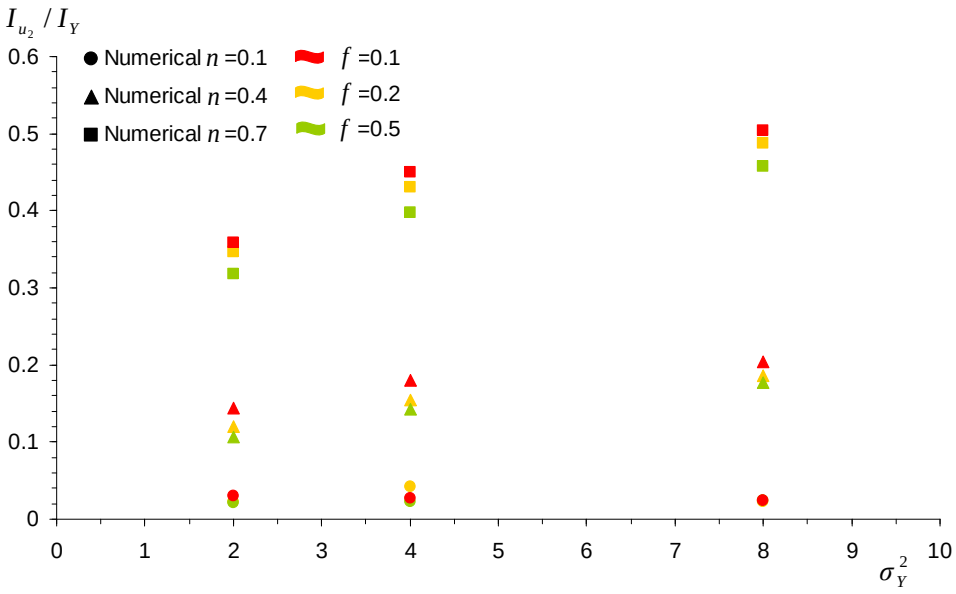

Figure 5.9: Longitudinal integral scale of transverse velocity (I_{u_2}), as function of the logconductivity variance σ_Y^2, for a few values of the anisotropy ratio f and the density n. Numerical Simulations (dots).

previous findings on ρ_{11}, and it confirms the robustness of the SC approach in modeling the longitudinal velocity statistics. The theoretical, first-order result for isotropic media $I_{u_1} = 15/8 I_Y$ is also represented in the Figure. It is seen that for anisotropic media the longitudinal velocity integral scale increases with the degree of heterogeneity, represented by σ_Y^2.

Things are different for the transverse (I_{u_2}) and vertical (I_{u_3}) integral scales (Figures 5.9,5.10). The SC result is identically $I_{u_2} = I_{u_3} = 0$, i.e. the transverse and vertical velocity covariances along x_1 are both hole-type covariances. However, the numerical results (dots) exhibit significant deviations from zero for the largest densities, lying in the same range as the values

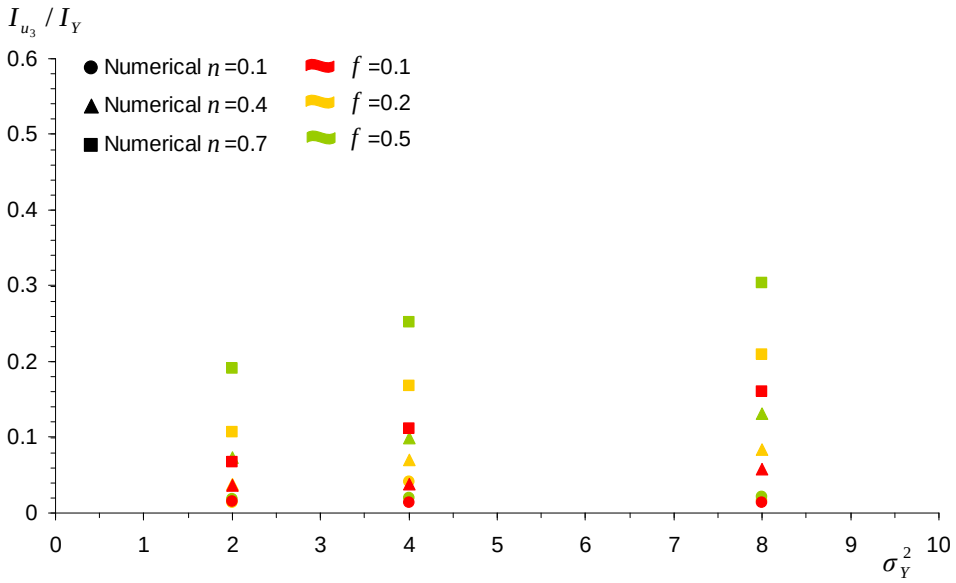

Figure 5.10: Longitudinal integral scale of vertical velocity (I_{u3}) as function of the logconductivity variance σ_Y^2, for a few values of the anisotropy ratio f and the density n. Numerical Simulations (dots).

for I_{u_1} in some cases. Russo et al. (1995 and 1998) found that when the mean flow is not aligned with the principal direction the integral scale of transverse and vertical velocity are not null within the FO approximation. Here, though the flow is aligned with the principal direction of anisotropy a significant correlation of V_2, V_3 along the horizontal direction may be found in dense, heterogeneous systems. This may have consequences on solute transport, providing a significant contribution at the transverse and vertical macrodispersivity. This is indeed what was found by Attinger et al. (2004), and Janković et al. (2009) by theoretical considerations and accurate 3D numerical simulations. The SC approach cannot model such feature which

strongly depends on the nonlinear inclusion interactions that manifest at large densities and are neglected in the present theoretical analysis.

Chapter 6

Transport

6.1 Overview

In this section we derive the approximate solution of transport by using the same procedure as we did for the effective hydraulic conductivity and the velocity statistics for heterogeneous anisotropic formations. To this aim the Lagrangian study of Fiori et al. (2003 and 2006) on the solute transport in highly heterogeneous isotropic formation is extended to anisotropic formations.

A flow uniform in the mean takes place through an heterogeneous anisotropic formation. A thin plume of uniform mass distribution is instaneously injected at $t = 0$ over a generic section of the flow domain $x_1 = -L$. We assume that the solute does not react with the matrix of the medium, and the flow properties are not influenced by the presence of the solute. The processes of local diffusion are neglected and the model developed here is fully dispersive. The injection zone is much larger than the integral scales in order to ensure the erogodicity of the problem. The solute is sampled in a section of the flow

domain $x_1 = L$. The solute flux $\mu(t, x)$ in the samplig section constitutes the Breakthrough curve (BTC). The BTC allows a more detailed description of the transport properties than the sintetic statistical parameters and it is a useful tool to understanding physical processes evolving in the medium. The approach employed has some similarities with other existing methods based on the time domain random walk framework, however, the main difference relies on the solution of the flow equation for a given formation from which the solution of the transport follows in a straightforward manner and calibration is not required. The approximate solutions shall be compared with the results of the numerical simulations developed by Prof. Igor Janković, details of numerical procedure are in Suribhatla et al. (2011).

6.2 Breakthrough Curve in the Self-Consistent Approximation

The transport is analized in the Lagrangian framework by the tracing of the singles tajectories of the solute particles. We fix our attention on a single particle that moves through the Multi-Indicator (MI) formation from the control plane in $x_1 - L$ to the control plane in $x_1 = L$. During its travel the particle crosses a large number of inclusions of different random hydraulic conductivity K_j. The traveltime of the domain can be obtained as the summation of the single traveltimes necessary to cross the M inclusions encountered by the particle

$$\tau(x) = \sum_{i=1}^{M} T_i \tag{6.1}$$

Along the same outline as in previous sections we develop the semi-

analytic study by using the Self-Consitent (SC) approximation, hence the study starts from the transport past an isolated inclusion of generic hydraulic conductivity K in a uniform matrix of hydraulic conductivity $\mathbf{K}_{ef}$. The coordinate system is placed in the centroid of the inclusion $\overline{\mathbf{x}}$, with the x_1 axis alligned with the principal direction of anisotropy. The expressions of the velocities developed in the previous section (2) are given in oblate spheroidal coordinates in Appendix A. The motion of the plume released in the section $x_1 = -L$ at $t = 0$ is described in terms of tajectories $\mathbf{x} = X(t; -L, b, k)$ where $b = \sqrt{(x_2 - \overline{x}_2)^2 + (x_3 - \overline{x}_3)^2}$ is the transverse radial coordinate. For a sufficient large time the plume stabilizes its shape translates with velocity U. The residual $X_D(b, k) = \lim_{t->+\infty}(X - Ut)$ is indipendent of time i.e. and is used in order to characterize the dipersion (Fiori et al., 2006). The asymptotic travel time residuals ar τ_R is derived from the equation

$$\tau_R(b, k) = 2\left(\lim_{L->+\infty}\int_0^L \frac{1}{V_1(x_1; \rho_t, k)}dx_1 - \frac{L}{U}\right) \tag{6.2}$$

where $\rho_t = \rho_t(x)$ is the equation of one single streamline originating at $\rho_t = b$ and $x_1 = -L$, $k = K/K_{efh}$ and V_1 is the longitudinal component of the velocity vector. In other words $\tau_R = X_D/U$, the delay or the advance of the traveltime of a particle with respect to the mean time becomes indipendent on L for large L . The derivation of τ_R requires a numerical integration and it can be split into the two components pertaining to the inside and the outside the spheroid.

$$\tau_M = \tau_M^{(in)} + \tau_M^{(ex)} \tag{6.3}$$

$$\tau_M^{(in)} \frac{U}{R_h} = \int_{-R_h}^{R_h} \frac{d(x/R_h)}{1 + u^{(in)}/U} - 2 \tag{6.4}$$

$$\tau_M^{(ex)} \frac{U}{R_h} = 2 \lim_{L->+\infty} \left(\int_{R_h}^{L} \frac{d(x/R_h)}{1 + u^{(ex)}/U} - (\frac{L}{R_h} - 1) \right)$$

The maximum advance or delay τ_M pertains to the central stramline ($b = 0$). For K close to infimum ($k \to 0$), τ_M is dominated by the residual of the traveltime in the interior of the inclusion that tends to infinity. Conversely, for $k \to \infty$ the residual traveltime, limited by the presence of the matrix, tends to a finite value. This asymmetry of X_D and hence of τ_R is the key to understanding the shape of the BTC curves and their long tails.

Fiori and Dagan, (2003) found that for a spherical inclusion, although the streamlines that do not cross the inclusion are influenced by its presence, their contribution to τ_R is negligible. The contributing streamlines which cross the oblate spheroidal inclusion are originated, in the plane $x_1 = -L$, from an ellipse of axis ratio $f_s = f\sqrt{K_{efh}/K_{efv}}$ and area A_L, related to the vertical section of the spheroid by the continuity equation:

$$\frac{A_L}{A_\omega} = \frac{V^{(in)}}{U} \tag{6.5}$$

where $A_\omega = \pi f_s R_h^2$ Furthermore, Fiori an Dagan, (2003) found that, for a spherical inclusion, the generic delay (or advance) τ_R can be expressed, in an approximate manner, in terms of the maximum delay (or advance) τ_M by the relathionship

$$\tau_R(\rho) = \tau_M \frac{l(\rho)}{2R_h} \tag{6.6}$$

where $l(\rho)$ is the length of segment of the streamline, generated in ρ, inside the spheroid.

If we assume, along the self-consistent approximation, that the residuals are indipendent we can determine them separately. Standing $x = 2L >> R_h$ we can adopt for the residuals the asymptotic expression, hence the traveltime becomes

$$\tau(x) = T + \sum_{i=1}^{M} \tau_{R,i} \tag{6.7}$$

with

$$\langle \tau(x) \rangle = T = \frac{x}{U} \tag{6.8}$$

The randomness of $\tau_{R,i}$ stems from two indipendent factors, the position of the particle at time t_0 in the area A_L and in the value of the conductivity ratio of the inclusions k_i. Conditioning on a fixed value of the k_i, makes the randomness of the trajectory within the sphere, manifests as randomness of the segment of crossing l. Assuming that the particle originates at equal probability from any point $x_{L,23}$ within A_L, the same is true for any point in A_ω and we obtain for the pdf of a generic $x_{\omega,23}$ point in A_ω from (6.5) the pdf

$$p(x_{\omega,23}) = \frac{V^{(in)}}{U} \frac{1}{A_\omega} \tag{6.9}$$

the pdf of ρ is

$$\begin{aligned} p(\rho) = p(x_{\omega,23}(\rho)) \frac{\partial x_\omega}{\partial \rho} = \\ = \frac{V^{(in)}}{U} 2\pi R_h^2 f_s \rho \frac{1}{\pi R_h^2 f_s} = \\ = \frac{V^{(in)}}{U} 2\rho \end{aligned} \tag{6.10}$$

the final $p(l)$ is:

$$p(l) = f(\rho(l))\frac{\partial \rho}{\partial l} = \tag{6.11}$$
$$= \frac{V^{(in)}}{U}\frac{2l}{2R_h}\frac{1}{2R_h} =$$
$$= \frac{V^{(in)}}{U}\frac{l}{2R_h^2}$$

Summarizing:

$$p(\tau_R|k)d\tau_R = p(l)dl \tag{6.12}$$

$$\begin{aligned} p(\tau_R|k) &= \frac{V^{(in)}}{U}\frac{l}{2R_h^2}\frac{dl}{d\tau_R} = \\ &= 2\frac{V^{(in)}}{U}\frac{\tau_R}{\tau_M(k)|\tau_M(k)|} \end{aligned} \tag{6.13}$$

We can now derive the marginal pdf of τ_R. To this aim we first invert the relationship $\tau_M(k)$: $k = \eta(\tau_M)$; then by observing that for a given τ_R the contribution to the integral over k is different form 0 only for $|\tau_M| > |\tau_R|$ we get finally

$$p(\tau_R) = \int_0^{+\infty} p(\tau_R|k)f(k)dk \rightarrow \tag{6.14}$$

$$\rightarrow \begin{cases} \int_0^{\eta(\tau_R)} p(\tau_R|k)f(k)dk \\ \int_{\eta(\tau_R)}^{+\infty} p(\tau_R|k)f(k)dk \end{cases}$$

It can be shown that the mean of the residual τ_R is not null, resulting a drift, caused by the neglected impact of the inclusion presence on the

exterior streamlines. To restore the consistence the drift shall be subtracted from $T = x/U$ in the pdf of τ

$$drift = \langle \tau_R \rangle = \frac{2}{3} \int_0^{+\infty} \frac{V_1^{(in)}(k)}{U} \tau_M(k) f(k) dk \tag{6.15}$$

The complete travel time (6.7)in the SC apprimation is derived assuming the indipendence of the $\tau_{R,i}$. As a consequence, the pdf of τ is obtained by the multiple convolution of $f(\tau_R)$. The number of convolution M is a random number depending on the particular path of the solute particle. However, if x is larger than few integral scale we can assume

$$M = n\frac{x}{\langle l \rangle} = n\frac{3x}{4R_h} = n\frac{9x}{16I_{Y,h}} \tag{6.16}$$

For the ergodicity, the pdf of the particle residence time inside the domain bounded by the two plane $x_1 = -L$ and $x_1 = L$, constitutes the solute flux in the sampling section. The final expression for the residence time or BTC curve is:

$$p(x, \tau) = FT^{-1}(FT(p(\tau_R))^M) \tag{6.17}$$

where FT indicates the Fourier transform.

The asymptotic longitudinal macrodispersivity is calculated (see Fiori et al. 2006) as

$$\alpha_{L,eq} = n\frac{3}{16}\frac{U^2}{R_h} \int_0^{\infty} \frac{V^{(in)}}{U} \tau_M^2(k) p(k) dk \tag{6.18}$$

It is emphasized that $\alpha_{L,eq}$ depends only on σ_Y^2, and the transport is Fickian.

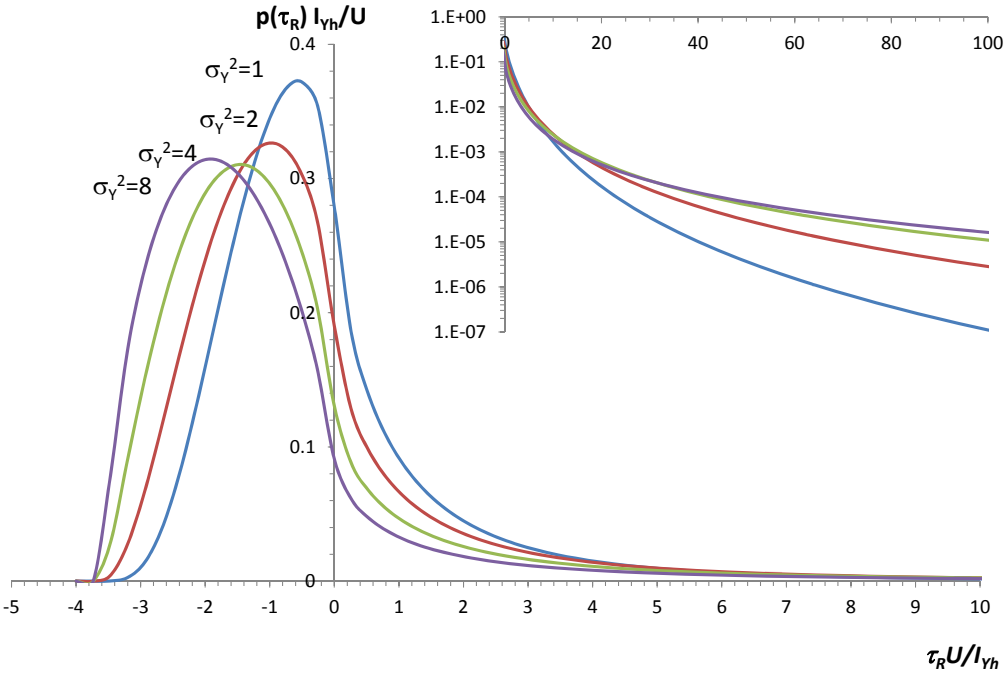

Figure 6.1: Distribution $p(\tau_R$ eq.(6.14) as function of τ_R for a few values of the logconductivity variance σ_Y^2 and for the anisotropy ratio $f = 0.1$.

The distribution of $p(\tau_R)$ represents the kernel of the system response in terms of transport dynamics. Figure 6.1 depicts $p(\tau_R)$ (6.14) as function of τ_R for different values of the logconductivity variance σ_Y^2. The results confirm the increasing of the asymmetry of the response $p(\tau_R)$ with σ_Y^2, as observed for isotropic structures in Fiori et al., (2003) and (2006).

Figure 6.2 shows, for a given variance ($\sigma_Y^2 = 4$) the increase of the asymmetry on the system response caused by the anisotropy. The anisotropy shifts the main bulk of the pdf toward the negative region, which represent the fast arrivals, in this case the shift is due to the fast inclusions ($Y/Y_G > 0$) that admit higher velocity values than the isotropic case. By contrast the

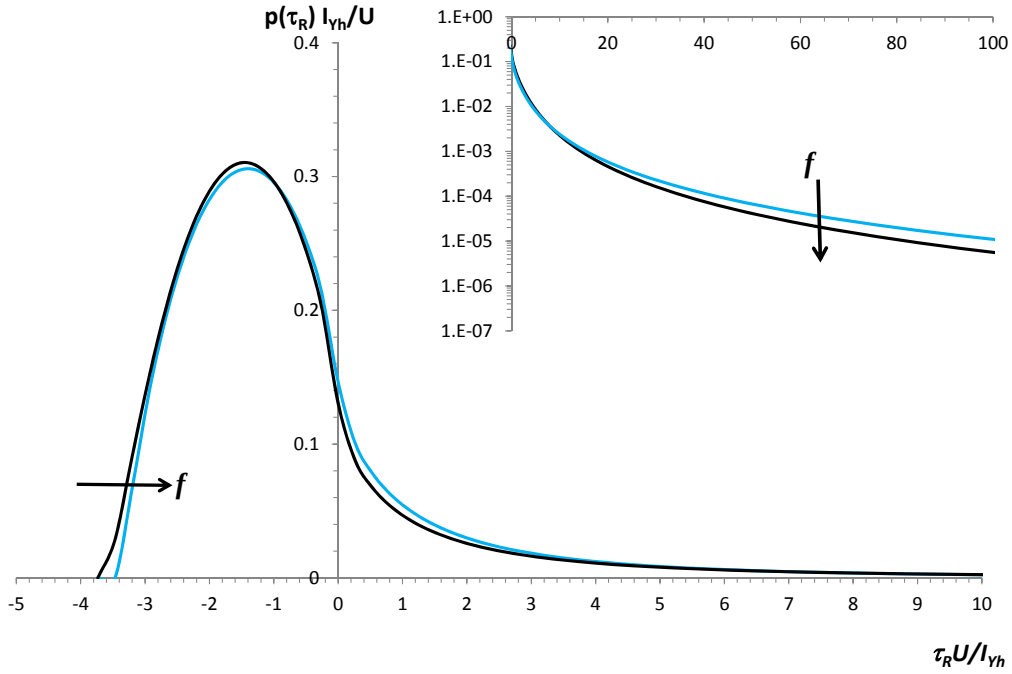

Figure 6.2: Distribution $p(\tau_R$ eq.(6.14) as function of τ_R for two values of the anisotropy ratio $f = 1, 0.1$, logconductivity variance $\sigma_Y^2 = 4$.

distribution of the late arrivals display a prolongation of the particle residence time inside the domain, that manifests its presence in the long tails of the τ_R distribution. Physically we can immagine that the anisotropy, as the heterogeneity, increases the activation of fast preferential channels in which the velocity is high and the particles move rapidly, on the other hand slow areas are created, in those zones the solute particles are trapped for long time.

We may conclude that for the kernel, the increase of the anisotropy results in the enhancement of the asimmetry of the traveltime distribution with a sort of separation between the fast and the late arrivals. The latter results

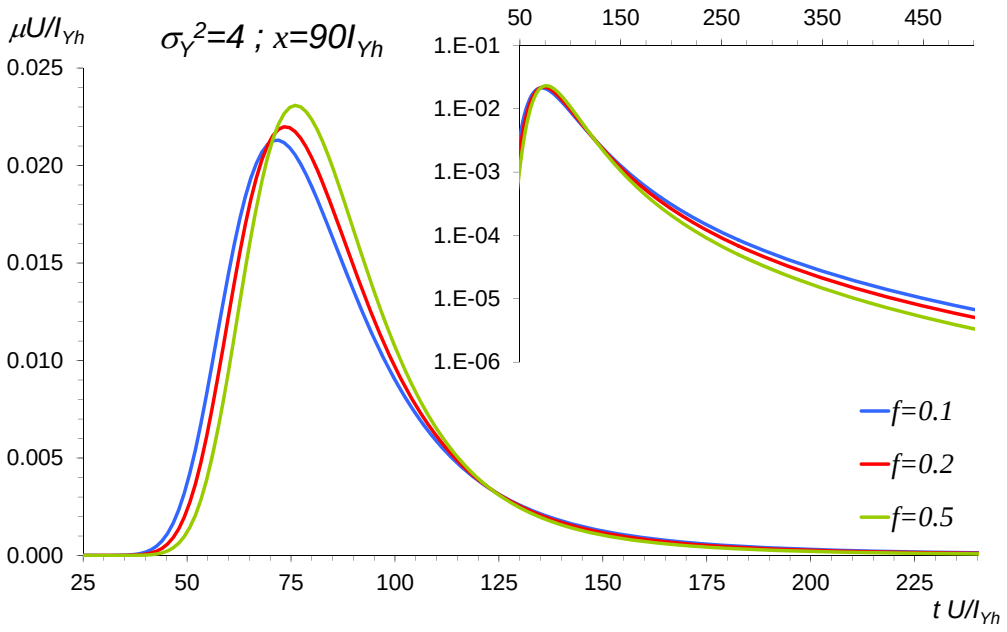

Figure 6.3: Solute flux $\mu(t;x)$ (equation (6.17) as function of time for three values of the anisotropy ratio $f = 0.1, 0.2, 0.5$, logconductivity variance $\sigma_Y^2 = 4$, domain dimension $x = 90 I_{Yh}$.

in a persistent tailing of $p(\tau_R)$ which causes a significant departure from the Gaussian solution of the transport eq(3.22).

We represent in Figure 6.3, the solute flux $\mu(t, x_1)$ as function of time t for a control plane $x = 90 I_{Yh}$, for $\sigma_Y^2 = 4$ and for different anisotropy f, we observe that μ shows a significant difference to the normal distribution emphasizing its non-Gaussian behavior, the asymmetry and the tailing increase with the anisotropy.

6.3 Results and Discussion

The first results shown in Figures 6.4,6.5, 6.6, displaying the dimensionless $\mu(t, x_1)\, I_{Y,h}/U$ as function of $tU/I_{Y,h}$ for $f = 0.1, 0.2, 0.5$ and for fixed values of $\sigma_Y^2 = 2, 4, 8$ and control plane position $x/I_{Y,h} = 90$ obtained through the SC approximation (lines) and throught numerical simulations (dots).

The numerical simulations are reproduced accurately by the SC model in low anisotropic media ($f = 0.5$), for all the tested σ_Y^2, however, the model accuracy decreases drastically when it is applied to anisotropies encountered in the natural porous formations. FOr these values of anisotropy significant differences in the BTCs obtained by SC model and by the numerical simulation can be observed in both the fast arrival and in the tail: SC model overpredicts the residence time of the solute inside the domain and, on the other hand, does not catch the peak of the BTC. In contrast to what was found for the $\mathbf{K}_{ef}$ and for the velocity statistics in anisotropic domain the SC model is unable to reproduce the numerical simulations, unlike the accuracy achieved for isotropic media.

However numerical simulations show low sensivity of the BTC for this reason we further investigated through the comparison of the numerical BTC obtained in anisotropic domains and the isotropic semi-analytical model.

The results are illustrated by Figures 6.7,6.8,6.9,6.10,6.11 displaying the dimensionless $\mu(t, x)\, I_{Y,h}/U$ as function of $tU/I_{Y,h}$ for $f = 0.1, 0.2, 0.5$ and for fixed values of $\sigma_Y^2 = 2, 4, 8$ and control plane positions $x/I_{Y,h} = 5, 10, 25, 50, 90$.

The large time tail is displayed on a logarithmic scale in the insert of each figure. The curve pertaining to $f = 1$ (isotropic media) was derived by the semi analytical model, developed by Fiori et al. (2006), which was found to be in excellent agreement with nuerical simlulations, as mentioned before.

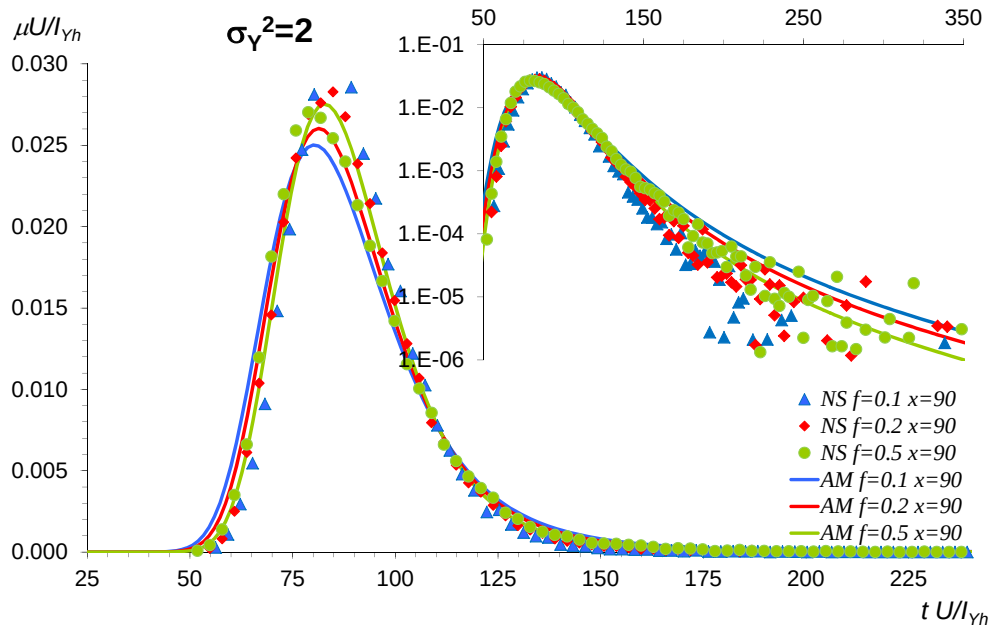

Figure 6.4: Solute flux $\mu(t;x)$ as function of time, comparison between AM: theoretical results (solid lines) and NS: numerical results (dots); solutions for three values of the anisotropy ratio $f = 0.1, 0.2, 0.5$, logconductivity variance $\sigma_Y^2 = 2$, domain dimension $x = 90 I_{Yh}$.

The striking finding displayed in Figures is the lack of dependence of the BTC upon the anisotropy factor $f = I_{Yv}/I_{Yh}$, except for some differences in the tail which somehow indicate a smaller mass for high anistropy. In words, transport in anisotropic media as quantified by the mass flux, does not differ from the one in isotropic media, for same σ_Y^2 and horizontal longconductivity integral scale I_{Yh}. Due to the simple relationship between the mass flux $\mu = \partial/\partial t\, [M(t, x_1)/M_0]$ and the plume longitudinal spatial mass distribution $m(x_1, t) = \int\int C(x_1, x_2, x_3)\, dx_2\, dx_3 = \partial/\partial x_1 [M(t, x_1)/M_0]$, where C is the concentration, it can be concluded that, for ergodic plumes, the average

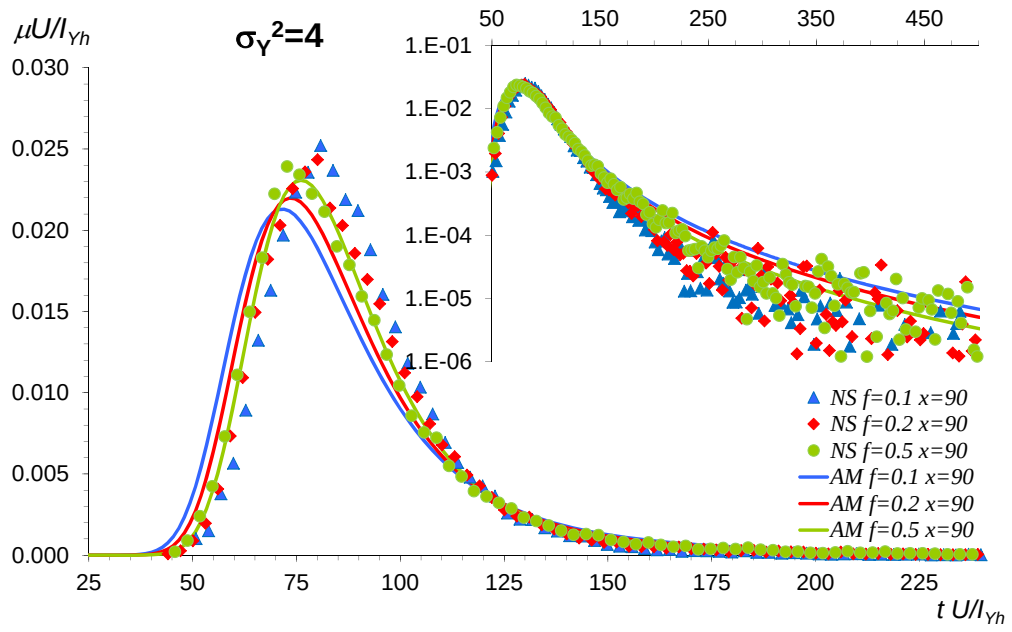

Figure 6.5: Solute flux $\mu(t;x)$ as function of time, comparison between AM: theoretical results (solid lines) and NS: numerical results (dots); solutions for three values of the anisotropy ratio $f = 0.1, 0.2, 0.5$, logconductivity variance $\sigma_Y^2 = 4$, domain dimension $x = 90 I_{Yh}$.

mass spatial distribution is insensitive to the anisotropy ratio as well.

This somehow unexpected and important result simplifies tremendously the modeling of transport in highly heterogeneous formations of axisymmetric anistropic structure, as far as the mass arrival and the transversally averaged concentration distribution are concerned. In particular the temporal and spatial moments, including the longitudinal macrodispersivity defined with the aid of the second moment, are not affected by anisotropy and can be determined with the aid of the simple approximate semi analytical methodology developed for spherical inclusions.

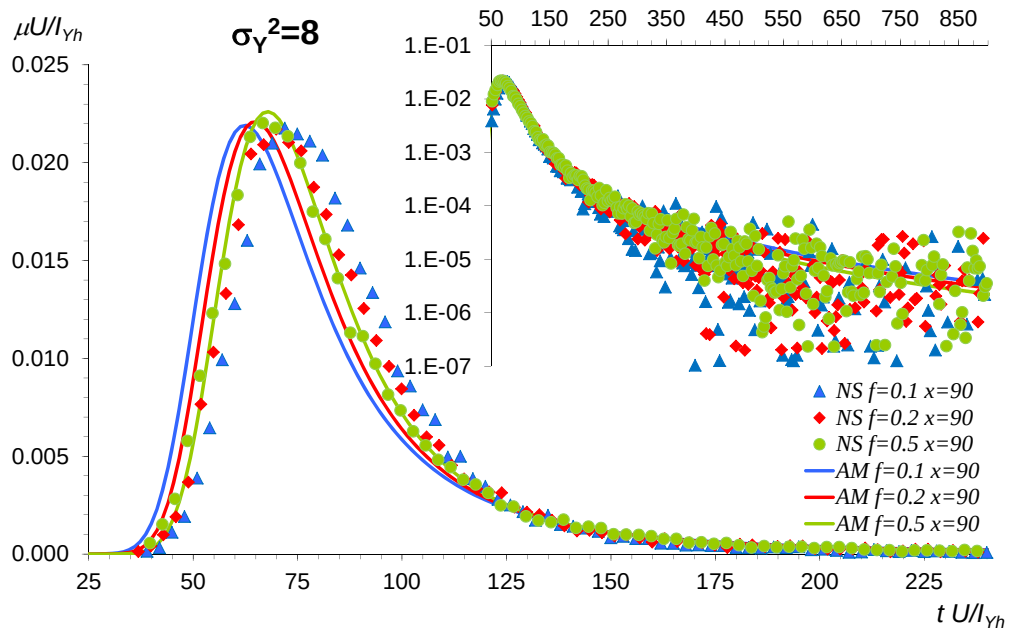

Figure 6.6: Solute flux $\mu(t;x)$ as function of time, comparison between AM: theoretical results (solid lines) and NS: numerical results (dots); solutions for three values of the anisotropy ratio $f = 0.1, 0.2, 0.5$, logconductivity variance $\sigma_Y^2 = 8$, domain dimension $x = 90 I_{Yh}$.

This result is in variance with the ones concerning the effective conductivity (Suribhatla et al., 2011) and the velocity variance (Zarlenga et al., 2012) for which f is quite influential. It is worthwhile to mention that a similar picture applies to weakly heterogeneous formations as modeled at first order in σ_Y^2 : K_{ef} and $u_{ij} = \langle u_i(\mathbf{x}) u_j(\mathbf{x}) \rangle$ (see e.g. *Dagan,* 1989 Fig. *3.4.4)* depend on f, whereas asymptotic transport is characterized by the macrodispersivity $\alpha_L = \sigma_Y^2 I_h$ for any f (Dagan, 1989 Fig. 4.6.1-4.6.4).

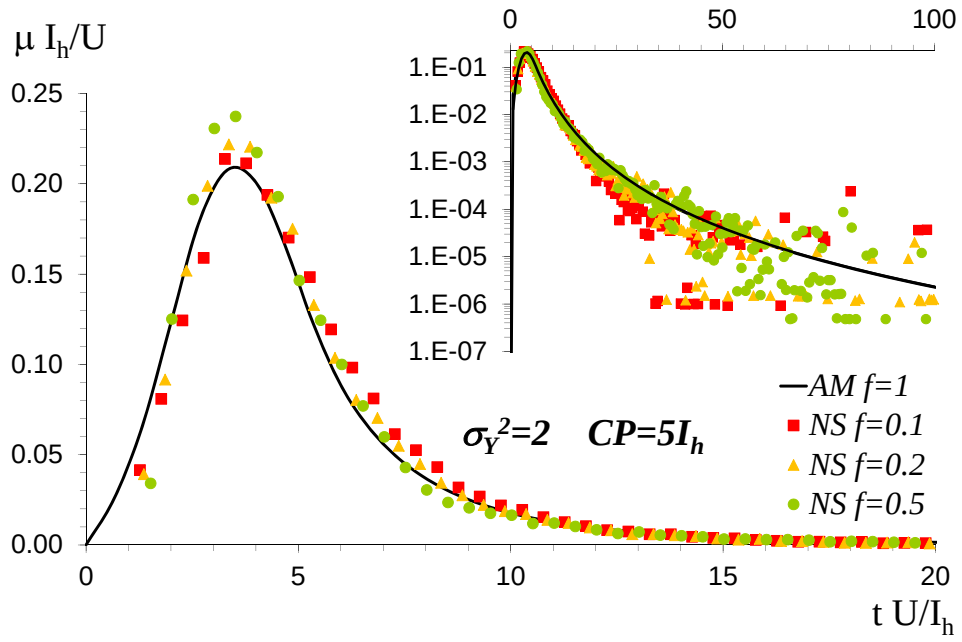

Figure 6.7: Solute flux $\mu(t;x)$ as function of time, comparison between theoretical result obtained for isotropic media (solid line) $f = 1$ and numerical results (dots) obtained for three values of the anisotropy ratio $f = 0.1, 0.2, 0.5$. Logconductivity variance $\sigma_Y^2 = 4$, domain dimension $x = 5I_{Yh}$.

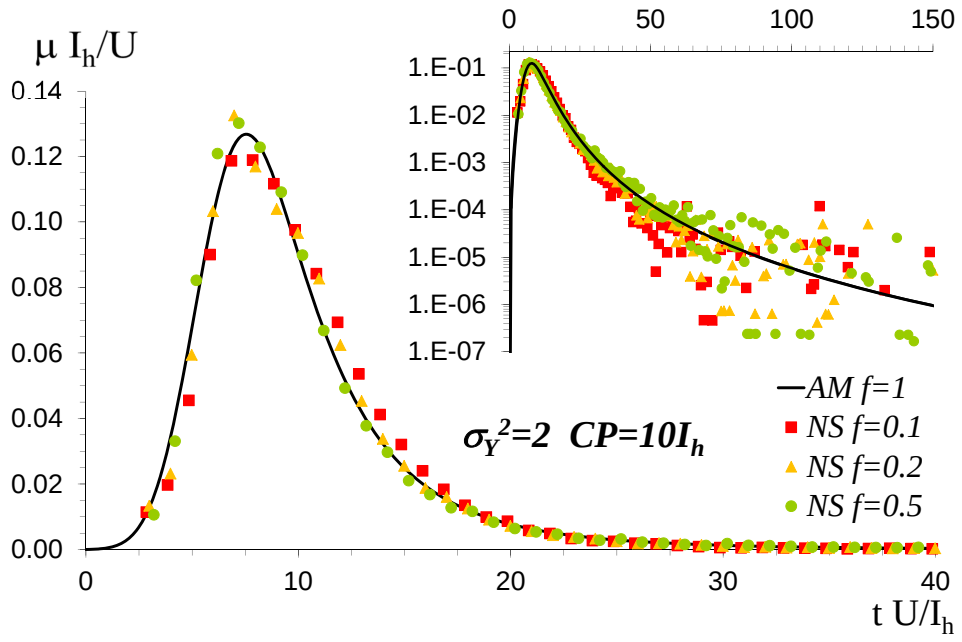

Figure 6.8: Solute flux $\mu(t;x)$ as function of time, comparison between theoretical result obtained for isotropic media (solid line) $f = 1$ and numerical results (dots) obtained for three values of the anisotropy ratio $f = 0.1, 0.2, 0.5$. Logconductivity variance $\sigma_Y^2 = 4$, domain dimension $x = 10I_{Yh}$.

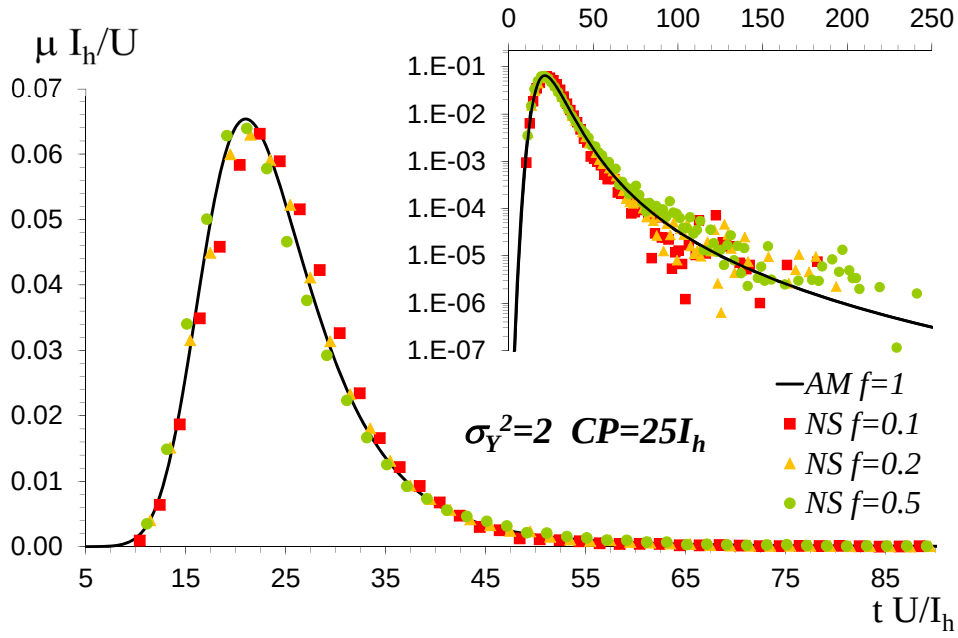

Figure 6.9: Solute flux $\mu(t;x)$ as function of time, comparison between theoretical result obtained for isotropic media (solid line) $f = 1$ and numerical results (dots) obtained for three values of the anisotropy ratio $f = 0.1, 0.2, 0.5$. Logconductivity variance $\sigma_Y^2 = 4$, domain dimension $x = 25 I_{Yh}$.

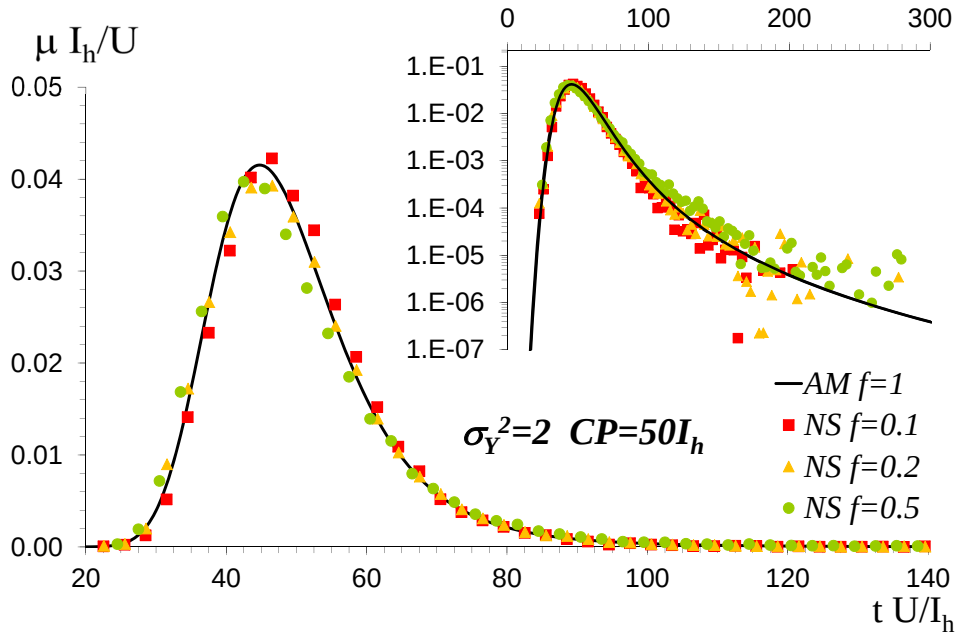

Figure 6.10: Solute flux $\mu(t;x)$ as function of time, comparison between theoretical result obtained for isotropic media (solid line) $f = 1$ and numerical results (dots) obtained for three values of the anisotropy ratio $f = 0.1, 0.2, 0.5$. Logconductivity variance $\sigma_Y^2 = 4$, domain dimension $x = 50 I_{Yh}$.

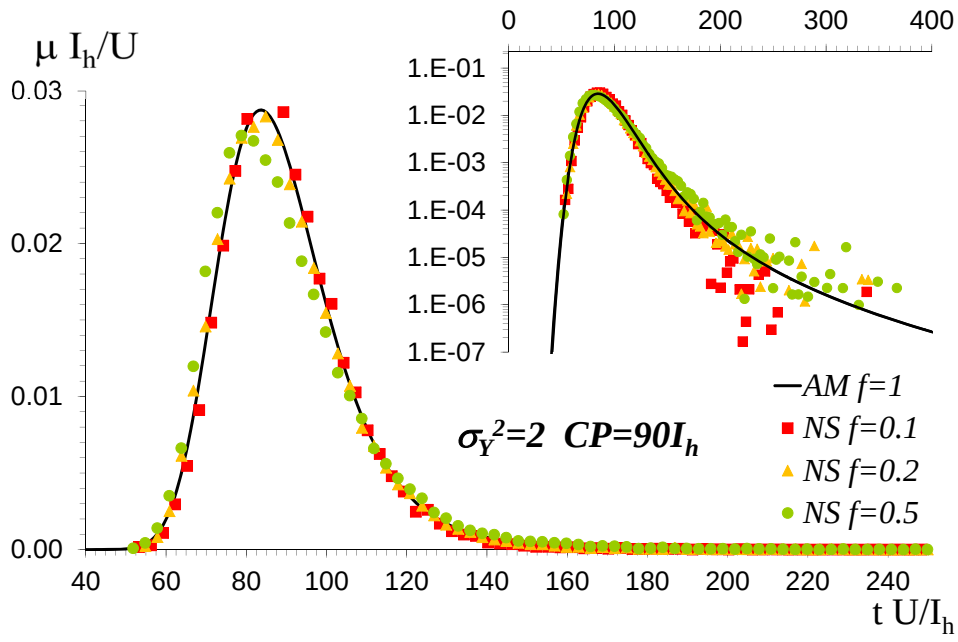

Figure 6.11: Solute flux $\mu(t;x)$ as function of time, comparison between theoretical result obtained for isotropic media (solid line) $f = 1$ and numerical results (dots) obtained for three values of the anisotropy ratio $f = 0.1, 0.2, 0.5$. Logconductivity variance $\sigma_Y^2 = 4$, domain dimension $x = 90 I_{Yh}$.

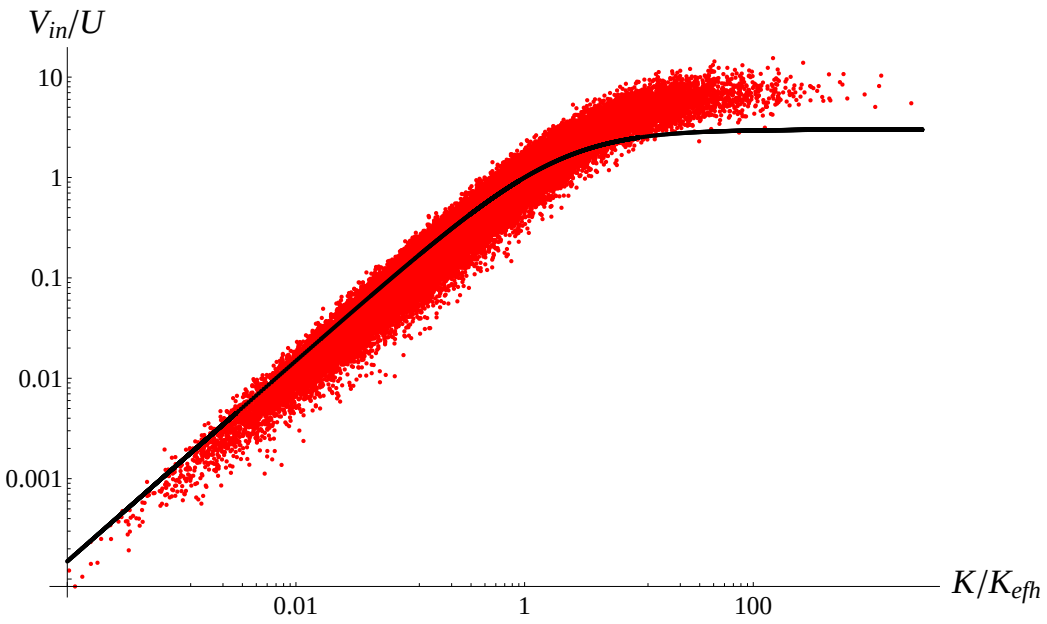

Figure 6.12: Longitudinal velocity inside the spheroid $V_1^{(in)}$ as function of the permeability ratio, theoretical result obtained for isotropic media (solid line) $f = 1$ and Numerical Results (dots) obtained for anisotropy ratio $f = 0.1$. Logconductivity variance $\sigma_Y^2 = 4$.

Chapter 7

Conclusions

In the present study an analytical method is developed for the analysis of several aspects of the flow and transport in a anisotropic heterogeneous porous formation. The main focus is on strongly heterogeneous formations, with large logconductivity variances σ_Y^2. The model is based on the Self-Consistent (SC) formulation of flow, which was previously developed for isotropic formations by Dagan et al., (2003), Fiori et al. (2003) and (2006), Jankovic et al., (2003). The approach is here extended to the more relevant case of anisotropic media. A Multi Indicator (MI) model, alternative to the common Multi-Gaussian ones, is adopted to conceptualize the medium. Through the MI approach an heterogeneous porous formation is modeled by a collection of blocks of constant conductivity K_i; a further approximation leads to considering blocks as inclusions of regular shapes. The inclusions occupy a fraction n of the medium, and the remaining $(1-n)$ fraction represents a conductivity field with correlation length much smaller than that of the inclusions (i.e. a nugget). The flow is uniform in the mean, and its direction is aligned with the long axis of anisotropy. Approximate semi-analytical solutions to the

flow and transport problems are achieved through the Self-Consitent (SC) approximation, for an ensemble of inclusions of lognormal conductivity distribution submerged in a matrix of effective conductivity $\mathbf{K}_{ef}$. SC approach makes the solution depend only on the flow and transport through an isolated inclusion of permeability K immersed in a matrix of anisotropic conductivity $\mathbf{K}_0$.

The results obtained through the SC approximation were compared with those obtained by the well-know First-Order (FO) approximation and with accurate numerical simulation (NS). Quantities analyzed are the effective hydraulic conductivity, the statistics of velocity and Breakthrough Curves (BTC). Numerical simulations were carried out by the prof. Jgor Jankovic using the procedure described in Suribhatla et al. (2011).

Analysis of the effective hydraulic conductivity of the medium.

In this study, beside the SC and FO models, the model known as Landau-Matheron exponential conjecture (LM) was introduced. The SC solution has a long tradition in the physics literature and was first implemented in the hydrological field by Dagan, (1981); the FO is a well-known solution formally valid for $\sigma_Y^2 \ll 1$, the exponential conjecture attempts to generalize the FO approximation for large σ_Y^2; a similar relation was formerly conjectured by Landau and Lifshitz, (1960) in electrodynamics and by Matheron, (1967) for isotropic porous media. The main contribution in this field stems in the comparisons between the results of the three analytical models and the numerical simulations.

An excellent agreement was found between the numerical simulation and the SC results: while the SC model is highly accurate for small densities, it slightly underestimates the effective conductivity only for the largest density ($n = 0.7$), and the discrepancy somehow increases with the degree of

heterogeneity. The dependence of the effective conductivity tensor $\mathbf{K}_{ef}$ on the degree of heterogeneity σ_Y^2 and on the anisotropy f reveals that the SC solution is very accurate for a broad range of parameters σ_Y^2 and f. In contrast, the FO solution strongly deviates from the numerical simulations for large σ_Y^2, as expected. The exponential conjecture seems unable to correctly represent the effective conductivity, especially for high heterogeneity. It was already found in the past that the exponential conjecture applicability is dependent on the covariance structure of the medium. The accuracy of SC method is proved by the accurate prediction of the interior velocity achieved by the solution of flow in the dilute medium approximation.

Analysis of the statistics of velocity.

The estimation of the velocity moments by the SC model is obtained by analytical expressions which require simple numerical quadratures.

It is seen that the effect of anisotropy is to increase the variance of the longitudinal velocity and reduce that of the transverse and vertical components. The trends are similar to those predicted by the first-order theory, which however generally overpredicts the velocity variance; the growth of the velocity variance with heteroeneity is usually less than linear. It is observed that the growth of the vertical velocity variance with heterogeneity σ_Y^2 is not always monotonous, and the variance may decrease after a certain σ_Y^2 threshold, as function of the degree of anisotropy f.

Analysis of the skewness and kurtosis suggests that the velocity pdf is generally far from Gaussian, except for weakly heterogeneous formations, when $\sigma_Y^2 \ll 1$. The deviation from Gaussianity is stronger for increasing anisotropy for all velocity components. The probability density functions (pdf) of the transverse and vertical velocities is approximately symmetrical, i.e. the skewness is zero in all cases, but the kurtosis is usually larger than

that pertaining to the Gaussian distribution.

Comparisons with numerical simulations, which are free from the assumptions made in the analytical model, indicate that the velocity variance is always well represented by the SC model for low density n. Even though this is not surprising, as the solution is based on the dilute approximation valid for $n \ll 1$, it is an important check of the analytical procedure. The SC solution deteriorates with increasing density and heterogeneity, as the nonlinear interactions (neglected in the analytical approach) between the inclusions become stronger. The effects of the interactions are not relevant for the longitudinal velocity, which is always well predicted by the SC method.

The velocity autocorrelation function $\rho_{mm}(r_s)$ modeled by the SC approach is weakly dependent on σ_Y^2, and this finding is confirmed by the numerical simulations. Also, the impact of the nonlinear interactions, which increase with the density n, is not overly significant for the longitudinal velocity autocorrelation function; the latter is always well captured by the SC model. It is seen that anisotropy leads to a general increase of the correlation, as also observed by the analysis of the velocity integral scales I_{u_m}. In turn, the transverse and vertical velocity integral scales are more influenced by the inclusion density, leading to positive values (the SC method predicts a hole-type covariance for both, i.e. zero integral scales) for high densities. In view of solute transport analysis, the result is consistent with the nonzero, and sometimes significant, transverse and vertical macrodispersivities found in other studies (e.g., Janković et al., 2009).

Analysis of the breakthrough curves.

The traveltime pdf $p(x,t)$ is equal to the relative solute flux $\mu(x,t)$. To determine the formulation for the pdfs further simplifications are required: the distribution of the residual traveltime τ_R of a thin plume moving over a

single inclusion is approximated in terms of the one on the central streamline τ_M; the total traveltime is the sum of the independent τ_{Ri} associated with inclusions encountered by a solute particle; the number of such inclusions is deterministic and equal to its mean value M.

It is seen that the effect of anisotropy f predicted by the SC model is to increase the asymmetry of the BTC enhancing the non-Gaussian behavior of solute transport processes emphasized in the past, for isotropic formations, by Fiori et al. (2006). In contrast to what was found for the $\mathbf{K}_{ef}$ and for the velocity statistics, the numerical simulations are reproduced accurately by the SC model only in low anisotropic media ($f = 0.5$).

However the numerical predicted BTCs show lack of dependence on the anisotropy. In words, transport in anisotropic media as quantified by the mass flux, does not differ from the one in isotropic media, for same σ_Y^2 and horizontal longconductivity integral scale I_{Yh}. It can be concluded that the average mass spatial distribution is insensitive to the anisotropy ratio f as well.This important finding allows drastic simplifications on the solute transport problem. However, the cancellation of the effect of anisotropy on transport in highly heterogeneous media still awaits a quantitative proof.

.

Appendix A

Velocity disturbance for an isolated spheroid

The calculation of the velocity moments is developed here by employing *the* oblate spheroidal coordinates. This coordinate system allows a mathematical simplification of velocity relations obtained for an isolated inclusion. The cartesian coordinates (x_s, y_s, z_s) are related to oblate spheroidal coordinates $(\zeta_s, \eta_s, \psi_s)$ by

$$\begin{aligned} x_s &= R\sqrt{1-f_s^2}\sqrt{(\zeta_s^2+1)\,(1-\eta_s^2)}\cos\psi_s \\ y_s &= R\sqrt{1-f_s^2}\sqrt{(\zeta_s^2+1)\,(1-\eta_s^2)}\sin\psi_s \\ z_s &= R\sqrt{1-f_s^2}\zeta_s\eta_s \end{aligned} \tag{A.1}$$

with

$$0 \le \zeta_s < \infty \;\; ; \;\; 1 \le \eta_s < 1 \;\; ; \;\; \pi \le \psi_s < \pi$$

For $\zeta_s = f_s/\sqrt{1-f_s^2} = const$ the previous equations describe in the cartesian space an oblate spheroid with axis ratio f_s and principal axis R. The potential disturbance in spheroidal coordinates is obtained by substituting

(A.1) in (3.57), leading to

$$\frac{\varphi^{(in)}}{UR} = C\left(f_s,k\right)\frac{\left(\zeta_0 - \left(1+\zeta_0^2\right)\cot^{-1}\zeta_0\right)}{2\left(1+\zeta_0^2\right)}\sqrt{\left(1-\eta_s^2\right)\left(1+\zeta_s^2\right)}\cos\psi_s \tag{A.2}$$

$$\frac{\varphi^{(ex)}}{UR} = C\left(f_s,k\right)\frac{\left(\zeta_s - \left(1+\zeta_s^2\right)\cot^{-1}\zeta_s\right)}{2\left(1+\zeta_s^2\right)}\sqrt{\left(1-\eta_s^2\right)\left(1+\zeta_s^2\right)}\cos\psi_s \tag{A.3}$$

where

$$C\left(f_s,k\right) = \frac{(k-1)}{1+A_0\left(k-1\right)}\frac{f_s}{\left(1-f_s^2\right)} \tag{A.4}$$

The velocity disturbance $\mathbf{u} = \nabla\varphi$ is obtained by derivation of (A.2) and (A.3), employing the relation for the derivatives in the cartesian directions under spheroidal coordinates (see, e.g., Zeppenfeld, 2009), the final result being

$$\frac{u_1^{(in)}}{U} = \frac{\left(k-1\right)\left(1-A_0\right)}{1+\left(k-1\right)A_0} \tag{A.5}$$

$$\frac{u_2^{(in)}}{U} = 0 \tag{A.6}$$

$$\frac{u_3^{(in)}}{U} = 0 \tag{A.7}$$

$$\frac{u_1^{(ex)}}{U} = C\left(f_s,k\right)\frac{\zeta_s\left(1+\zeta_s^2+\left(1-\eta_s^2\right)\cos\left(2\psi_s\right)\right) - \left(1+\zeta_s^2\right)\left(\zeta_s^2+\eta_s^2\right)\cot^{-1}\zeta_s}{2\left(1+\zeta_s^2\right)\left(\zeta_s^2+\eta_s^2\right)} \tag{A.8}$$

$$\frac{u_2^{(ex)}}{U} = C\left(f_s,k\right)\frac{\zeta_s\left(1-\eta_s^2\right)\cos\psi_s\sin\psi_s}{\left(1+\zeta_s^2\right)\left(\zeta_s^2+\eta_s^2\right)} \tag{A.9}$$

$$\frac{u_3^{(ex)}}{U} = C\left(f_s,k\right)\frac{\eta_s\sqrt{1-\eta_s^2}\cos\psi_s}{\sqrt{1+\zeta_s^2}\left(\zeta_s^2+\eta_s^2\right)} \tag{A.10}$$

Appendix B

Proof of Eq. (5.6)

The general expression of the velocity covariance is given by (5.5), which is rewritten here for convenience

$$u_{ms}\left(\mathbf{x}-\mathbf{y}\right)=\left\langle \sum_{j=1}^{N}\sum_{k=1}^{N}u_{j,m}\left(\mathbf{x}-\bar{\mathbf{x}}_{j};K_{j}\right)u_{k,s}\left(\mathbf{y}-\bar{\mathbf{x}}_{k};K_{k}\right)\right\rangle \tag{B.1}$$

where the dependence on the hydraulic conductivity is made explicit.

The contribution of the different terms $u_{j,m}\left(\mathbf{x}-\bar{\mathbf{x}}_{j}\right)u_{k,s}\left(\mathbf{y}-\bar{\mathbf{x}}_{k}\right)$ is split between the off-diagonal terms (i.e., for $j\neq k$) and the diagonal ones ($j=k$). We average first the generic off-diagonal term over the independent random variables $\bar{\mathbf{x}}_{k}$,K_{k}, of pdf equal to $1/\Omega$, $f\left(K_{k}\right)$, respectively

$$u_{j,m}\left(\mathbf{x}-\bar{\mathbf{x}}_{j};K_{j}\right)\frac{1}{\Omega-\omega_{j}}\int\limits_{\Omega-\omega_{j}}\int u_{k,s}\left(\mathbf{y}-\bar{\mathbf{x}}_{k};K_{k}\right)f\left(K_{k}\right)dK_{k}d\bar{\mathbf{x}}_{k} \tag{B.2}$$

where the integration over the domain $\Omega-\omega_{j}$ is because of the non-overlap

condition. The integration in (B.2) is split as follows

$$\begin{aligned} & \frac{1}{\Omega-\omega_j}\int\limits_{\Omega-\omega_j}\int u_{k,s}\left(\mathbf{y}-\bar{\mathbf{x}}_k;K_k\right)f\left(K_k\right)dK_k d\bar{\mathbf{x}}_k \qquad \text{(B.3)} \\ = \; & \frac{1}{\Omega-\omega_j}\int\limits_{\Omega}\int u_{k,s}\left(\mathbf{y}-\bar{\mathbf{x}}_k;K_k\right)f\left(K_k\right)dK_k d\bar{\mathbf{x}}_k - \\ & -\frac{1}{\Omega-\omega_j}\int\limits_{\omega_j}\int u_{k,s}\left(\mathbf{y}-\bar{\mathbf{x}}_k;K_k\right)f\left(K_k\right)dK_k d\bar{\mathbf{x}}_k \\ = \; & -\frac{1}{\Omega-\omega_j}\int\limits_{\omega_j}\int u_{k,s}\left(\mathbf{y}-\bar{\mathbf{x}}_k;K_k\right)f\left(K_k\right)dK_k d\bar{\mathbf{x}}_k \end{aligned}$$

where the identity (5.3) has been employed. In the limit **of** $\omega_j/\Omega \to 0$ the above term becomes very small and negligible in comparison with the diagonal ones; hence, the off-diagonal terms do not contribute in (B.1), and we are left only with the contribution of the diagonal terms, i.e.

$$\begin{aligned} & \left\langle u_{j,m}\left(\mathbf{x}-\bar{\mathbf{x}}_j\right)u_{k,s}\left(\mathbf{y}-\bar{\mathbf{x}}_k\right)\right\rangle \qquad \text{(B.4)} \\ = \; & \frac{1}{\Omega}\int\limits_{\Omega}\int u_{j,m}\left(\mathbf{x}-\bar{\mathbf{x}}_j;K_j\right)u_{k,s}\left(\mathbf{y}-\bar{\mathbf{x}}_j;K_j\right)f\left(K_j\right)dK_j d\bar{\mathbf{x}}_j \end{aligned}$$

The latter is inserted in (B.1), yielding at the limit $\Omega \to \infty$

$$u_{ms}\left(\mathbf{x}-\mathbf{y}\right)=\sum_{j=1}^{N}\frac{1}{\Omega}\int\limits_{\Omega}\int u_{j,m}\left(\mathbf{x}-\bar{\mathbf{x}}_j;K_j\right)u_{k,s}\left(\mathbf{y}-\bar{\mathbf{x}}_j;K_j\right)f\left(K_j\right)dK_j d\bar{\mathbf{x}}_j \qquad \text{(B.5)}$$

Performing in (B.5) a change of variables and employing the relation $N\omega = n\Omega$ leads to the final expression (5.6).

Bibliography

[1] Bellin, A., P. Salandin, and A. Rinaldo, Simulation of Dispersion in Heterogeneous Porous Formations: Statistics, First-Order Theories, Convergence of Computations, *Water Resour. Res.,* 28(9), 2211-2227, doi:10.1029/92WR00578, 1992.

[2] Boggs, J. M., S. C. Young, and L. M. Beard, Field study of dispersion in a heterogeneous aquifer: 1. Overview and site description, *Water Resour. Res.*, 28, 3281– 3291, 1992.

[3] Burr, D., E. Sudicky, and R. Naff, Nonreactive and reactive solute transport in three-dimensional heterogeneous porous media: Mean displacement, plume spreading, and uncertainty, *Water Resour. Res.,* 30(3), 791-815, doi:10.1029/93WR02946, 1994.

[4] Carslaw, H.S., and J.C. Jaeger, *Conduction of Heat in Solids,* Oxford Univ. Press, 1959.

[5] Chin, D., and T. Wang, An Investigation of the Validity of First-Order Stochastic Dispersion Theories in Isotropie Porous Media, *Water Resour. Res.,* 28(6), 1531-1542, doi:10.1029/92WR00666, 1992.

[6] de Dreuzy, J.-R., A. Beaudoin, and J. Erhel, Asymptotic dispersion in 2D heterogeneous porous media determined by parallel numerical simulations, *Water Resour. Res.*, 43, W10439, doi:10.1029/2006WR005394, 2007.

[7] Deng, F.-W., and J.H. Cushman, On higher order corrections to the flow velocity covariance tensor, revisited, *Water Resour. Res.,* 34(1), 103-106, doi:10.1029/97WR02610, 1998.

[8] Dagan, G., Models of Groundwater Flow in Statistically Homogeneous Porous Formations, *Water Resour. Res.,* 15(1), 47-63, doi:10.1029/WR015i001p00047, 1979.

[9] Dagan, G., Analysis of Flow Through Heterogeneous Random Aquifers by the Method of Embedding Matrix. Part 1: Steady Flow, *Water Resour. Res.,* 17(1), 107-121, doi:10.1029/WR017i001p00107, 1981.

[10] Dagan, G., Theory of solute transport by groundwater, *Ann. Rev. Fluid Mech., 1987.19:183:215,* 1987

[11] Dagan, G., *Flow and Transport in Porous Formations*, Springer-Verlag, Heidelberg, 465 p., 1989.

[12] Dagan, G., A. Fiori, Time-dependent transport in heterogeneous formations of bimodel structures: 1. The model, *Water Resour. Res.,* 39, 1112, doi:10.1029/2002WR001396, 2003

[13] Dagan, G., A. Fiori, I. Janković. Flow and transport in highly heterogeneous formations. Part 1: Conceptual framework and validity of first-order approximations, *Water Resour. Res.,* 39, 1268, doi:10.1029/2002WR001717, 2003.

[14] Eames, I., and J. W. M. Bush, Longitudinal dispersion by bodies fixed in a potential flow, *Proc. R. Soc. Lond. A*, vol. 455, no.1990, 3665-3686, doi:10.1098/rspa.1999.0471, 1999.

[15] Englert, A., J. Vanderborght, and H. Vereecken, Prediction of velocity statistics in three-dimensional multi-Gaussian hydraulic conductivity fields, *Water Resour. Res.*, 42 , W03418, doi:10.1029/2005WR004014, 2006.

[16] Fiori, A., and G. Dagan, Concentration fluctuations in aquifer transport: a rigorous first-order solution and application, J. Contam. Hydrol., 45 (2000) 139-163, doi:/10.1016/S0169-7722(00)00123-6, 2000

[17] Fiori, A., and G. Dagan, Time-dependent transport in heterogeneous formations of bimodel structures: 1. Results, *Water Resour. Res.,* 39, 1125, doi:10.1029/2002WR001398, 2003

[18] Fiori, A., I. Janković, and G. Dagan, Flow and Transport in Highly Heterogeneous Formations. Part 2. Semianalytical results for isotropic media, *Water Resour. Res.*, 39, 1269, doi:10.1029/2002WR001719, 2003.

[19] Fiori, A., I. Janković, and G. Dagan, Modeling flow and transport in highly heterogeneous three-dimensional aquifers: Ergodicity, Gaussianity, and anomalous behavior. Part 2: Approximate semianalytical solution , *Water Resour. Res.* , 42 , W06D13, doi:10.1029/2005WR004752, 2006.

[20] Fiori, A., G. Dagan, I. Janković. Upscaling of Steady Flow in Three-Dimensional Highly Heterogeneous Formations. MMS flow upscaling paper, *Multiscale Model. Simul.*,,2011

[21] Fitts, C. R., Modeling three-dimensional flow about ellipsoidal inhomogeneities with application to flow to a gravel-packed well and flow through lens-shaped inhomogeneities, Water Resour. Res., 27, 815 –824, 1991.

[22] Freeze, R. A. 1975, A Stochastic-Conceptual Analysis of One-Dimensional Groundwater Flow in Nonuniform Homogeneous Media, *Water Resour. Res.*, 11, 5, doi:10.1029/WR011i005p00725, 1975

[23] Gelhar, L. J., and C. L. Axness, Three-dimensional stochastic analysis of macrodispersion in aquifers, *Water Resour. Res.*, 19, 161– 180, 1983.

[24] Gelhar, L. J., *Stochastic susurface Hydology*, Prentice Hall, Englewood Cliffs, New Jersery, 390 p., 1993.

[25] Gómez-Hernández, J.J., and X.-H. Wen, To be or not to be multi-Gaussian? A reflection on stochastic hydrogeology., *Adv. Water Resour.,* 21 (1), 47 – 61, doi:10.1016/S0309-1708(96)00031-0, 1996.

[26] Gotovac, H., V. Cvetkovic, and R. Andricevic, Flow and travel time statistics in highly heterogeneous porous media , *Water Resour. Res.*, 45, W07402, doi:10.1029/2008WR007168, 2009.

[27] Hsu, K.-C., D. Zhang, and S. Neuman, Higher-Order Effects on Flow and Transport in Randomly Heterogeneous Porous Media, *Water Resour. Res.*, 32, 3, doi:10.1029/95WR03492, 1996.

[28] Hsu, K.-C., and S. Neuman, Second-Order Expressions for Velocity Moments in Two- and Three-Dimensional Statistically Anisotropic Media, *Water Resour. Res.*, 33(4), 625-637*,* doi:10.1029/97WR00045, 1997.

[29] Janković, I. and R. Barnes, Three-Dimensional Flow Through Large Numbers of Spheroidal Inhomogeneities, *Journal of Hydrology*, 226(3-4), 225-234, 1999

[30] Janković, I., A. Fiori and G. Dagan, Effective Conductivity of an Isotropic Heterogeneous Medium of Lognormal Conductivity Distribution, *Multiscale Modeling, Analysis, and Simulation* (MMAS), 1(1), 40-56, 2003

[31] Janković, I., A. Fiori, and G. Dagan, Flow and Transport in Highly Heterogeneous Formations. Part 3: Numerical simulations and comparison with theoretical results, *Water Resour. Res.*, 39, 1270, doi:10.1029/2002WR001721, 2003.

[32] Janković, I., A. Fiori, and G. Dagan, Modeling flow and transport in highly heterogeneous three-dimensional aquifers: Ergodicity, Gaussianity, and Anomalous Behavior. Part 1: Conceptual issues and numerical simulations, *Water Resour. Res.*, 42 , W06D12, doi:10.1029/2005WR004734, 2006.

[33] Janković, I., D. R. Steward, R. J. Barnes, and G. Dagan, Is transverse macrodispersivity in three-dimensional groundwater transport equal to zero? A counterexample, *Water Resour. Res.*, 45, W08415, doi:10.1029/2009WR007741, 2009.

[34] Kitanidis, P.K., Introduction to Geostatistics: Applications in Hydrogeology. Cambridge, U.K.: Cambridge University Press.,1997.

[35] Milton, G.W., *Theory of composites*, Oxford Univ. Press, 2002.

[36] Nowak, W., R. L. Schwede, O. A. Cirpka, and I. Neuweiler, Probability density functions of hydraulic head and velocity in three dimensional heterogeneous porous media, *Water Resour. Res.*, 44, W08452, doi:10.1029/2007WR006383, 2008.

[37] Rehfeldt, K. R., J. M. Boggs, and L. W. Gelhar, Field study of dispersion in a heterogeneous aquifer 3. Geostatistical analysis of hydraulic conductivity, *Water Resour. Res.*, 28, 3309 – 3324.,1992.

[38] Renard, P., and G. de Marsily. 1997. Calculating equivalent permeability: A review. *Adv. Water Resour* 20, doi: 10.1016/S0309-1708(96)00050-4, 1997.

[39] Rubin, Y., *Applied Stochastic Hydrogeology*, Oxford Univ. Press, 2003.

[40] Rubin, Y., and G. Dagan, A Note on Head and Velocity Covariances in Three-Dimensional Flow Through Heterogeneous Anisotropic Porous Media, *Water Resour. Res.*, 28(5), 1463-1470, doi:10.1029/92WR00107, 1992.

[41] Russo, D., On the Velocity Covariance and Transport Modeling in Heterogeneous Anisotropic Porous Formations. Part 1: Saturated Flow, *Water Resour. Res.*, 31(1), 129-137doi:10.1029/94WR01783, 1995.

[42] Russo, D., A note on the velocity covariance and transport modeling in partially saturated heterogeneous porous formations of two- and three-dimensional structures, *Adv. Water Resour.,* 21: 251-258, doi:10.1016/S0309-1708(96)00060-7, 1998.

[43] Salandin, P., and V. Fiorotto (1998), Solute Transport in Highly Heterogeneous Aquifers, *Water Resour. Res.*, 34(5), 949-961, doi:10.1029/98WR00219, 1998.

[44] Suribhatla, R., development and application of analytic element method for esimation of effective Hydraulic conductivity of anisotropic porous formations, PhD thesis, Faculty of the graduate school of the State University of New York at Buffalo, 2007.

[45] Suribhatla, R., I. Janković, A. Fiori, A. Zarlenga, and G. Dagan, Effective conductivity of anisotropic heterogeneous medium of random conductivity distribution,*Multiscale Model. Simul.,* 9, 933-954, 2011

[46] Torquato, S., *Random Heterogeneous Materials: Microstructure and Macroscopic Properties*, Springer-Verlag*,* 2002.

[47] Zhang, D., S. P. Neuman, Comment on "A Note on Head and Velocity Covariances in Three-Dimensional Flow Through Heterogeneous Anisotropic Porous Media" by Y. Rubin and G. Dagan, *Water Resour. Res.*, 28, 12, doi:10.1029/92WR02223, 1992.

[48] Zeppenfeld, M., Solutions to Maxwell's equations using spheroidal coordinates, *New J. Phys.,* 11, 073007, doi:10.1088/1367-2630/11/7/073007, 2009.